University of Nebraska - Lincoln
DigitalCommons@University of Nebraska - Lincoln

Andrzej Rajca Publications | Published Research - Department of Chemistry

2009

Noncovalent Interactions in the Asymmetric Synthesis of Rigid, Conjugated Helical Structures

Makoto Miyasaka
University of Nebraska - Lincoln

Maren Pink
Indiana University - Bloomington

Suchada Rajca
University of Nebraska-Lincoln, srajca1@unl.edu

Andrzej Rajca
University of Nebraska - Lincoln, arajca1@unl.edu

Follow this and additional works at: http://digitalcommons.unl.edu/chemistryrajca

Part of the Chemistry Commons

Miyasaka, Makoto; Pink, Maren; Rajca, Suchada; and Rajca, Andrzej, "Noncovalent Interactions in the Asymmetric Synthesis of Rigid, Conjugated Helical Structures" (2009). *Andrzej Rajca Publications*. 5.
http://digitalcommons.unl.edu/chemistryrajca/5

This Article is brought to you for free and open access by the Published Research - Department of Chemistry at DigitalCommons@University of Nebraska - Lincoln. It has been accepted for inclusion in Andrzej Rajca Publications by an authorized administrator of DigitalCommons@University of Nebraska - Lincoln.

Published in *Angewandte Chemie International Edition* 48:32 (2009), pp. 5954–5957; doi: 10.1002/anie.200901349
Copyright © 2009 WILEY-VCH Verlag GmbH & Co. KGaA, Weinheim. Used by permission.

The authors thank the National Science Foundation for support of this work through grants CHE-0414936 and CHE-0718117. ChemMatCARS Sector 15 is principally supported by the National Science Foundation/Department of Energy under grant number CHE-0535644. Use of the Advanced Photon Source was supported by the U.S. Department of Energy, Office of Science, Office of Basic Energy Sciences, under contract no. DE-AC02-06CH11357. Dr. Yu-Sheng Chen is thanked for help with data collection.

Submitted March 10, 2009; revised May 16, 2009; published online June 30, 2009

Noncovalent Interactions in the Asymmetric Synthesis of Rigid, Conjugated Helical Structures

Makoto Miyasaka,[1] Maren Pink,[2] Suchada Rajca,[1] and Andrzej Rajca [1]

1. Department of Chemistry, University of Nebraska–Lincoln, Lincoln, NE 68588-0304 USA
2. Department of Chemistry, IUMSC, Indiana University, Bloomington, IN 47405-7102 USA
Corresponding author — Andrzej Rajca, Department of Chemistry, University of Nebraska–Lincoln, Lincoln, NE 68588-0304 USA; fax 402 472-9402; email arajca1@unl.edu ; home page http://www.chem.unl.edu/rajca/rajcahome.html

Keywords: asymmetric synthesis, chirality, chiroptical properties, helical structures, helicenes

Helical supramolecular architecture, such as helical foldamers, supramolecular helicates and aggregates, helical molecules, macromolecules, and oligomers, is a fascinating topic of interest in chemistry and materials science.[1–6] Although such supramolecular structures may provide advantages in the design of stimuli-responsive and functional materials, the weak nature of the noncovalent forces, as well as the dependency of the dynamic process on their local environments, may hinder their possible applications because of their limited structural stability and processibility. Stabilization of these supramolecular structures could be achieved by modification of the molecular backbone with specific functional groups that permit intramolecular cross-linking, in which covalent bonds fix the secondary structure with variable degrees of fidelity.[6, 7]

Helical structures derived from conjugated *ortho*-annelated aromatic rings, known as [*n*]helicenes, are precisely defined at the molecular level.[8–11] For [*n*]helicenes with a sufficiently large number of aromatic rings (*n*), rigid conformations with large barriers to racemization and enhanced molecular chiroptical properties may be expected.[11a, 12, 13] Diverse electronic structures for such helices may result from various aromatic rings[11ab–19] or by introducing antiaromatic rings[20] to the structure, to obtain materials with a wide range of band gaps, 2-4 eV.[11a, 11b, 17, 20, 21]

Although significant progress has been made in the synthesis of [*n*]helicenes, the preparation of such highly annelated and strained π-systems,[11] especially by asymmetric synthesis,[16, 17, 22–24] remains a challenge. The development of new synthetic strategies for the preparation of precisely defined and extended helical structures, as well as understanding the factors that control the structure and properties of these molecules, are crucial to making progress in the area of rigid helical motifs.

Herein, we demonstrate the important role of noncovalent interactions in the asymmetric synthesis of rigid, conjugated helical structures. Tetrakis(β-trithiophene) **1** folds into a helical conformation that facilitates the double ring annelation to provide a carbon-sulfur bis[7]helicene **2** with a rigid, helically locked structure (Figure 1 a). Further ring annelation of the rigid, locked bis[7]helicene to form the corresponding [15]helicene **3** was not successful, likely owing to strong noncovalent interactions between the two [7]helicene moieties which prohibit their relative rotation to facilitate covalent bond formation, however, other effects may not be excluded.

We propose that the "helical fold-and-lock" concept may be extended to facilitate the preparation of the oligomers of [*n*]helicenes, such as tetrakis[7]helicene (Figure 1b). Such oligomers may provide precisely defined models for helical folding, which is driven by intramolecular π-stacking and steric repulsion.[1a]

The asymmetric synthesis of bis[7]helicene **2** is outlined in Scheme 1. The synthetic approach mostly follows the methodology for the iterative synthesis of carbon-sulfur [*n*]helicenes (*n* = 7 and 11) that we developed previously.[15–17] In the synthesis of long [*n*]helicenes, the isolation and purification of poorly soluble intermediates and products can be an arduous undertaking. We can circumvent solubility problems by using the large tripropylsilyl (TPS) group as a protecting group.

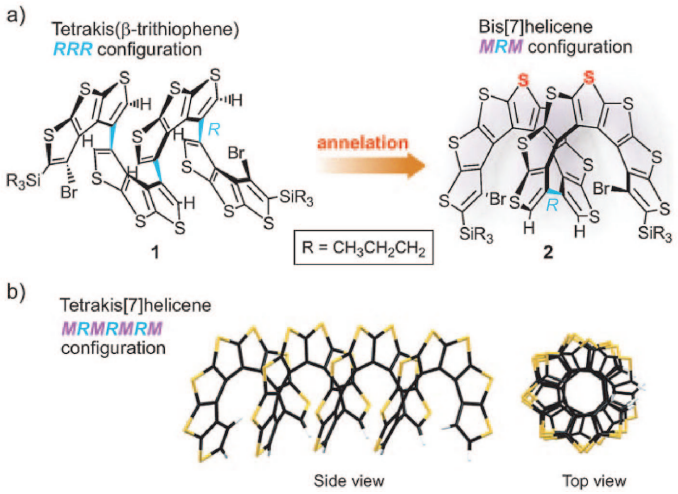

Figure 1. a) From helically folded tetrakis(β-trithiophene) to helically locked bis[7]helicene. b) Oligomer of [*n*]helicenes illustrated by tetrakis[7]helicene. *R* indicates the configuration of chiral axes and *M* indicates the configuration of "left-handed" [*n*]helicene moieties.

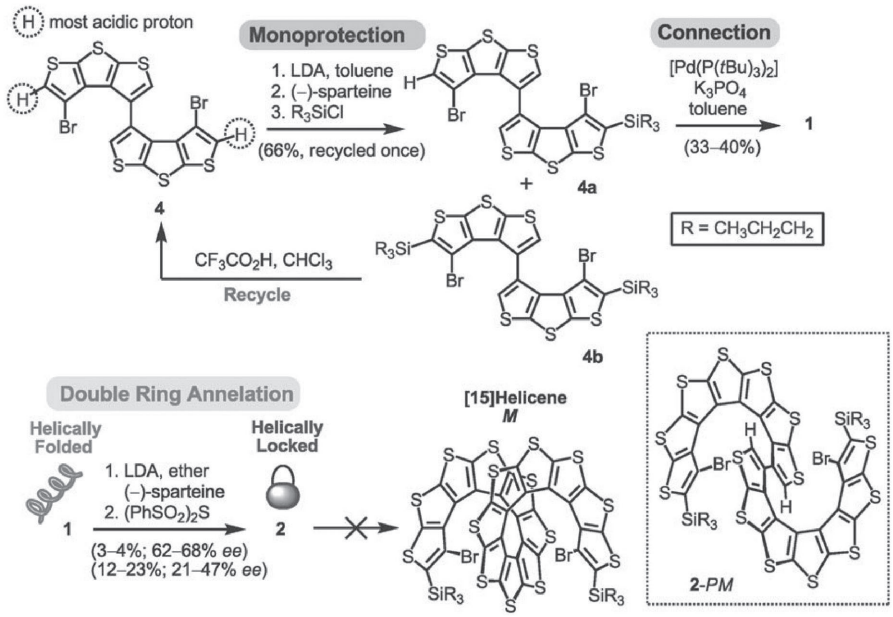

Scheme 1. Asymmetric synthesis of bis[7]helicene **2**. Inset: *meso*-diastereomer of bis[7]helicene.

In the first step, monoprotection of the two most acidic positions in bis(β-trithiophene) **4** yielded its derivative **4 a**, which had enhanced solubility and steric shielding at one of the CBr moieties.

The steric shielding provided selectivity in the palladium-catalyzed homocoupling reaction to form tetrakis(β-trithiophene) **1**, as carbon-carbon bond formation is preferred at the less sterically shielded CBr moiety. In the double ring annelation reaction, **1** is tetralithiated with lithium diisopropylamide (LDA) in the presence of a chiral diamine such as (-)-sparteine, and then treated with bis(phenylsulfonyl)sulfide ($(PhSO_2)_2S$) to form two new thiophene rings. The resultant bis[7]helicene **2** was obtained in approximately 20 % yield after isolation and had a modest enantiomeric excess (*ee*) value.[25] The isolated bis[7]helicene **2** is chiral, and therefore, its [7]helicene moieties are likely to possess identical configurations, for example *MM* or *PP*. An alternative *meso*-diastereomer, such as **2**-*PM*, with the [7]helicene moieties of the opposite configuration (*PM*) was not detected (Scheme 1, Inset).

The structures of tetrakis(β-trithiophene) **1** and bis[7]helicene **2** were determined by single-crystal X-ray analysis using synchrotron radiation (Figure 2).[26] Tetrakis(β-trithiophene) **1** crystallized in the nonchiral space group *C*2/*c* with half of the molecule in the asymmetric unit. Bis[7]helicene **2** crystallized in the chiral space group $C222_1$ with half of the molecule and half of a solvent molecule (benzene) in the asymmetric unit. The crystal of **2** was found to be merohedrally twinned with an enantiomeric ratio in the crystal of 88:12, which is consistent with the *ee* value of the bulk sample (Scheme 1).

In the X-ray structure, **1** adopts a C_2-symmetric conformation, with approximately planar annelated β-trithiophene moieties; the dihedral angles for the terminal-to-center and the center-to-center moieties are 83.28(3)° and 84.21(3)°, respectively. Notably, the chiral axes have the same configuration, *RRR* or *SSS*, at all three β,β-linkages, that is, the carbon-carbon bonds connect the annelated β-trithiophene moieties at the β-positions of the terminal thiophenes. The helical folding of **1**, which is likely driven by steric repulsion and pairwise π-stacking of the annelated β-trithiophene moieties, provides a preferred conformer for double ring annelation to form the two [7]helicene moieties in **2**, as illustrated in the space-filling models in Figure 2 c,d. Thus, the *RRR* (or *SSS*) configuration of **1** is converted into the *MRM* (or *PSP*) configuration in bis[7]helicene **2**. In the major enantiomer of **2**, *MRM*, the [7]helicene moieties possess the *M* configuration and the chiral axis at the β,β-linkage has the corresponding *R* configuration.

The conformation of **2** has an approximate C_2 point group of symmetry. The β,β-linkage, which has a torsion angle of approximately -50° about the carbon-carbon bond connecting the [7]helicene moieties, resemble a molecular hinge in which two rigid [7]helicene moieties form an intramolecular π-stack assembled in a helical motif. The short intramolecular distances on both sides of the molecular hinge lead to a rigid conformation (Figure 2 e, Table S1 in the Supporting Information).

In solution, racemic tetrakis(β-trithiophene) **1** possesses a chiral conformation on the time scale of enantiomer separation by both high pressure liquid chromatography (HPLC) and nuclear magnetic resonance (NMR) methods. The chiral conformation is indicated by well resolved peaks resulting from diastereomeric interactions with the chiral stationary phase of the HPLC column and interactions with chiral shift reagents in NMR experiments (see the Supporting Information). The conformation and electronic structure of chiral bis[7]helicene **2** in solution was further characterized by computational modeling of experimental circular dichroism (CD) and ultraviolet-visible (UV/Vis) spectra.

To gain deeper insight into the structure and properties of bis[7]helicene, we calculated a series of simplified structures, in which the large TPS group was replaced with a trimethylsilyl (TMS) group. Electronic CD and UV/Vis absorption spectra of bis[7]helicene **2 a**, [15]helicene **3 a**, and [7]helicene **5** were computed using the TD-B3LYP/6-31G(d) method and the IEF-PCM-UAHF solvent model for cyclohexane.[27–29] The calculated spectra are qualitatively similar for all three structures, especially for bis[7]helicene **2 a** and [15]helicene **3 a**, which both possess relatively weak long-wavelength bands. For bis[7]helicene **2 a** and [7]helicene **5**, excellent agreement between experiment and theory was found (Figure 3 and see the Supporting Information).

Specifically in **2** the weak, long-wavelength band with a positive Δε band at approximately 330 nm is qualitatively reproduced in the calculated spectrum (Figure 3, Inset). In [15]helicene **3 a**, this long-wavelength band shows a somewhat larger and negative Δε value, which may reflect the smaller torsion angles of about 14° between the two [7]helicene moieties (vs. 50° in bis[7]helicene) and the out-of-plane distortion of the thiophene rings near the center in [15]helicene (see the Supporting Information). We conclude that bis[7]helicene **2** adopts a [15]helicene-like rigid conformation in the solid state and in solution, and it possesses

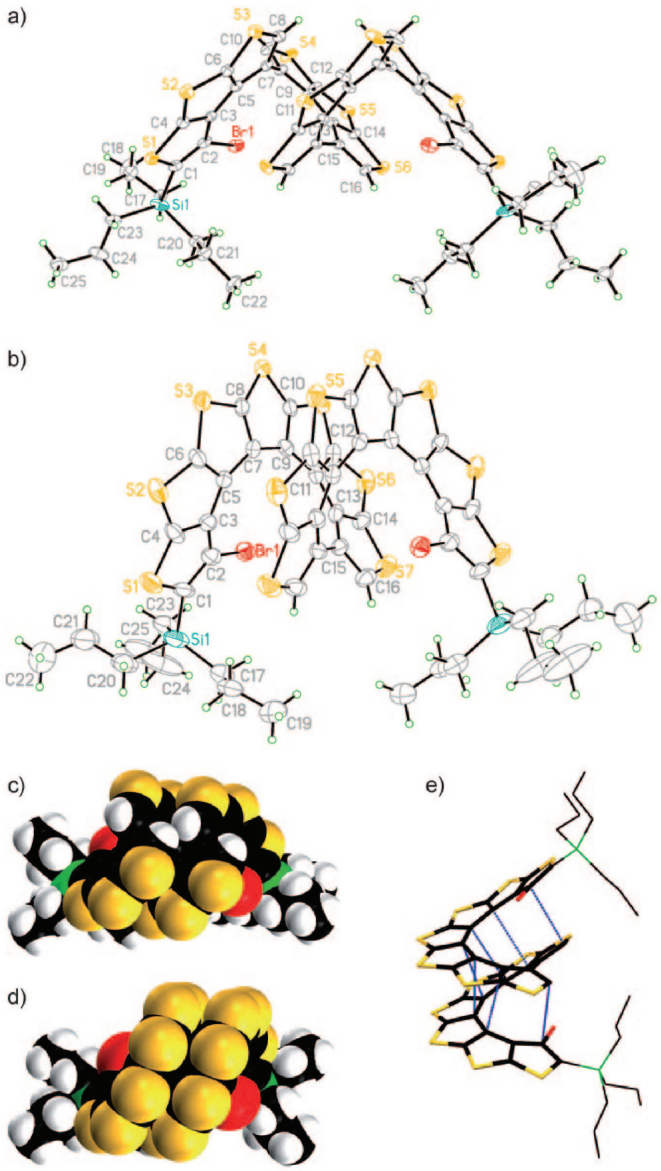

Figure 2. Molecular structure and conformation: a) tetrakis(β-trithiophene) **1**; b) bis[7]helicene **2**; c) space-filling model for **1**; d) space-filling model for **2**; e) short intramolecular C···C distances (3.23-3.30 Å) between the [7]helicene moieties in bis[7]helicene **2** are indicated with blue lines. ORTEP plots with thermal ellipsoids set at the 50 % probability level. Cocrystallized solvent and disorder in the propyl groups are omitted for clarity.

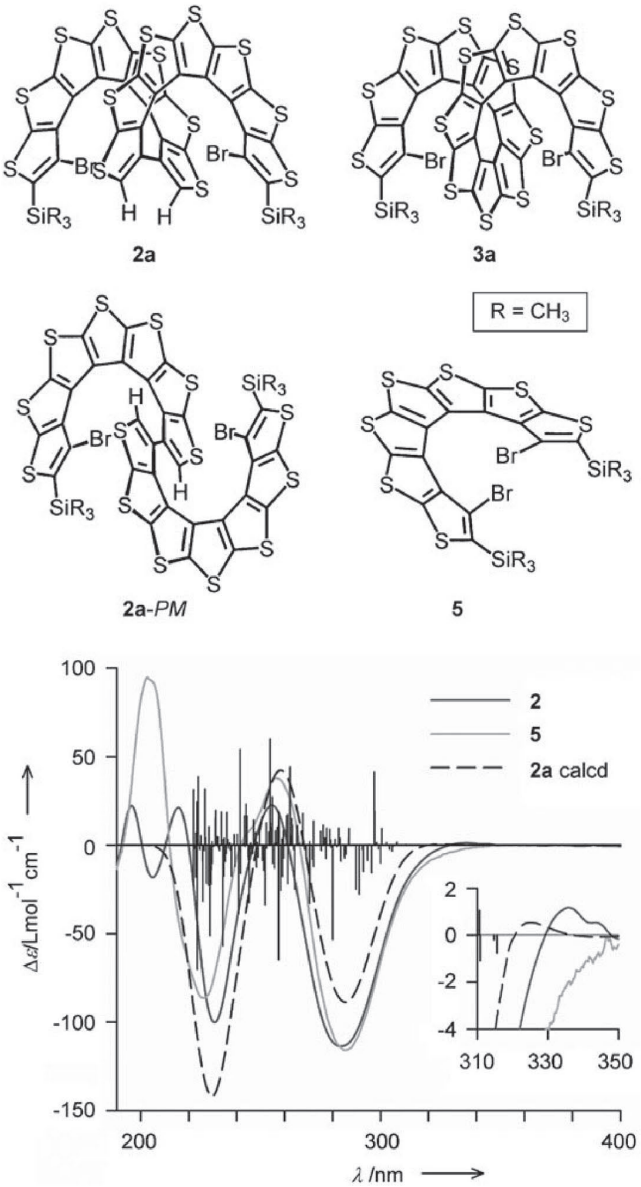

Figure 3. Experimental and calculated electronic CD spectra in cyclohexane. Inset: expansion of CD spectra.

an electronic structure similar to that for the corresponding [15]helicene.

We explored the isomerization of bis[7]helicene **2** into its *meso*-diastereomer (**2**-*PM*; Scheme 1), a process that corresponds to the inversion of one of the [7]helicene moieties. Under similar conditions that lead to the inversion (racemization) of [7]helicene **5**,[16] only the starting bis[7]helicene **2** was recovered. This result suggests that **2**, with *MM* or *PP* [7]helicene moieties, is thermodynamically preferred. Computational studies at the B3LYP/6-31(d) level of theory indicate that **2 a**-*PM* is about 8 kcal mol^{-1} higher in energy than **2 a**, which has the *MM* configuration. This energy difference is about the same for single point energy calculations using the IEF-PCM-UAHF solvent model for cyclohexane (see the Supporting Information). We attribute this energy preference to the strong noncovalent interactions - π-stacking in the helically folded diastereomer **2 a**.

We examined the correlation between molecular connectivity and helical folding by computational modeling. Model oligomers of [7]helicenes, analogues of bis[7]helicene **2 a** in which the bromine and TMS groups are replaced with hydrogen atoms, were studied at the B3LYP/6-31(d,p) level of theory.[27] A series of structures based on bis[7]helicenes, tris[7]helicenes, and tetrakis[7]helicenes, were constructed by connecting the [7]helicene moieties of identical (*MM*) or opposite (*MP*) configuration at each β,β-linkage. In this series, oligomers with identical configurations, such as *MM* at each linkage, have lower energies than those with *MP* configurations. This preference is about 5 to 8 kcal mol^{-1} for each β,β-linkage,

and tends to be larger for higher oligomers, probably as a result of steric factors. For example, the tetramer of [7]helicenes with identical configuration (*MMMM*) such as tetrakis[7]helicene in Figure 1b and **8**-*MMMM* (see Table S5 in the Supporting Information) is lower in energy by about 20 kcal mol^{-1} than the corresponding *meso*-diastereomer with *MPMP* configuration. In contrast, we found a reversed trend in analogous bis[7]helicenes with α,α-linkages, that is, the diastereomer with the [7]helicene moieties of opposite configuration is lower in energy,[27, 30] albeit the preference is quite small - about 1 kcal mol^{-1}.

We predict that a strong preference for helical folding, driven by intramolecular π-stacking and steric repulsion, may be realized in oligomers of [*n*]helicene monomers with the same configuration and which are connected at the inner rim of the [*n*]helicenes. For moderate values of *n*, such oligomers could provide extended rigid-rod helical structures that are precisely defined at the molecular level and are expected to possess enhanced chiral properties.

References

1. a) *Top. Curr. Chem.* (Eds.: M. Crego-Calama, D. N. Reinhoudt), 2006, *265*, pp. 1-312; b) *Foldamers: Structure, Properties and Applications* (Eds: S. Hecht, I. Huc), Wiley-VCH, Weinheim, 2007, pp. 1-448.
2. a) M. T. Stone, J. M. Heemstra, J. S. Moore, *Acc. Chem. Res.* 2006, **39**, 11-20; b) D. J. Hill, M. J. Mio, R. B. Prince, T. S. Hughes, J. S. Moore, *Chem. Rev.* 2001, **101**, 3893-4012.
3. H. Sugiura, Y. Nigorikawa, Y. Saiki, K. Nakamura, M. Yamaguchi, *J. Am. Chem. Soc.* 2004, **126**, 14858-14864.
4. E. Kolomiets, V. Berl, J.-M. Lehn, *Chem. Eur. J.* 2007, **13**, 5466-5479.
5. L. Trembleau, J. Rebek, Jr., *Science* 2003, **301**, 1219-1220.
6. S. Hecht, *Mater. Today*, March **2005**, pp. 48-55.
7. S. Hecht, A. Khan, *Angew. Chem.* 2003, **115**, 6203-6206; *Angew. Chem. Int. Ed.* 2003, **42**, 6021-6024.
8. M. S. Newman, D. Lednicer, *J. Am. Chem. Soc.* 1956, **78**, 4765-4770.
9. I. Pischel, S. Grimme, S. Kotila, M. Nieger, F. Vögtle, *Tetrahedron: Asymmetry* 1996, **7**, 109-116.
10. a) T. J. Katz, *Angew. Chem.* 2000, **112**, 1997-1999; *Angew. Chem. Int. Ed.* 2000, **39**, 1921-1923; b) K. E. S. Phillips, T. J. Katz, S. Jockusch, A. J. Lovinger, N. J. Turro, *J. Am. Chem. Soc.* 2001, **123**, 11899-11907.
11. Recent reviews: a) A. Rajca, M. Miyasaka in *Functional Organic Materials - Syntheses and Strategies*, (Eds.: T. J. J. Mueller, U. H. F. Bunz), Wiley-VCH, New York, 2007, Chapter 15, pp. 543-577; b) A. Rajca, S. Rajca, M. Pink, M. Miyasaka, *Synlett* 2007, 1799-1822; c) S. K. Collins, M. P. Vachon, *Org. Biomol. Chem.* 2006, **4**, 2518-2524; d) T. Torroba, M. García-Valverde, *Angew. Chem.* 2006, **118**, 8270-8274; *Angew. Chem. Int. Ed.* 2006, **45**, 8092-8096; e) A. Urbano, *Angew. Chem.* 2003, **115**, 4116-4119; *Angew. Chem. Int. Ed.* 2003, **42**, 3986-3989.
12. a) J. E. Field, G. Muller, J. P. Riehl, D. Venkataraman, *J. Am. Chem. Soc.* 2003, **125**, 11808-11809; b) Y. Tang, T. A. Cook, A. E. Cohen, *J. Phys. Chem. A* 2009, **113**, 6213-6216.
13. P. P. Meurer, F. Vögtle, *Top. Curr. Chem.* 1985, **127**, 1-76.
14. a) L. Adriaenssens, L. Severa, T. Šálová, I. Císařová, R. Pohl, D. Šaman, S. V. Rocha, N. S. Finney, L. Pospíšil, P. Slavíček, F. Teplý, *Chem. Eur. J.* 2009, **15**, 1072-1076; b) S. Graule, M. Rudolph, N. Vanthuyne, J. Autschbach, C. Roussel, J. Crassous, R. Réau, *J. Am. Chem. Soc.* 2009, **131**, 3183-3185; c) J. Míšek, F. Teplý, I. G. Stará, M. Tichý, D. Šaman, I. Císařová, P. Vojtíšek, I. Starý, *Angew. Chem.* 2008, **120**, 3232-3235; *Angew. Chem. Int. Ed.* 2008, **47**, 3188-3191; d) N. Takenaka, R. S. Sarangthem, B. Captain, *Angew. Chem.* 2008, **120**, 9854-9856; *Angew. Chem. Int. Ed.* 2008, **47**, 9708-9710; e) G. Lamanna, C. Faggi, F. Gasparrini, A. Ciogli, C. Villani, P. J. Stephens, F. J. Devlin, S. Menichetti, *Chem. Eur. J.* 2008, **14**, 5747-5750; f) J. Ichikawa, M. Yokota, T. Kudo, S. Umezaki, *Angew. Chem.* 2008, **120**, 4948-4951; *Angew. Chem. Int. Ed.* 2008, **47**, 4870-4873.
15. A. Rajca, H. Wang, M. Pink, S. Rajca, *Angew. Chem.* 2000, **112**, 4655-4657; *Angew. Chem. Int. Ed.* 2000, **39**, 4481-4483.
16. A. Rajca, M. Miyasaka, M. Pink, H. Wang, S. Rajca, *J. Am. Chem. Soc.* 2004, **126**, 15211-15222.
17. M. Miyasaka, A. Rajca, M. Pink, S. Rajca, *J. Am. Chem. Soc.* 2005, **127**, 13806-13807.
18. Y. Dai, T. J. Katz, *J. Org. Chem.* 1997, **62**, 1274-1285.
19. T. Iwasaki, Y. Kohinata, H. Nishide, *Org. Lett.* 2005, **7**, 755-758.
20. a) S. Han, A. D. Bond, R. L. Disch, D. Holmes, J. M. Schulman, S. J. Teat, K. P. C. Vollhardt, G. D. Whitener, *Angew. Chem.* 2002, **114**, 3357-3361; *Angew. Chem. Int. Ed.* 2002, **41**, 3223-3227; b) S. Han, D. R. Anderson, A. D. Bond, H. V. Chu, R. L. Disch, D. Holmes, J. M. Schulman, S. J. Teat, K. P. C. Vollhardt, G. D. Whitener, *Angew. Chem.* 2002, **114**, 3361-3364; *Angew. Chem. Int. Ed.* 2002, **41**, 3227-3230.
21. Y.-H. Tian, G. Park, M. Kertesz, *Chem. Mater.* 2008, **20**, 3266-3277.
22. a) M. C. Carreño, M González-López, A. Urbano, *Chem. Commun.* 2005, 611-613; b) M. C. Carreño, Á. Enríquez, S. García-Cerrada, M. J. Sanz-Cuesta, A. Urbano, F. Maseras, A. Nonell-Canals, *Chem. Eur. J.* 2008, **14**, 603-620.
23. a) S. K. Collins, A. Grandbois, M. P. Vachon, J. Côté, J. *Angew. Chem.* 2006, **118**, 2989-2992; *Angew. Chem. Int. Ed.* 2006, **45**, 2923-2926; b) A. Grandbois, S. K. Collins, *Chem. Eur. J.* 2008, **14**, 9323-9329.
24. a) F. Teplý, I. G. Stará, I. Starý, A. Kollárovič, D. Šaman, L. Rulíšek, P. Fiedler, *J. Am. Chem. Soc.* 2002, **124**, 9175-9180; b) P. Sehnal, Z. Krausová, F. Teplý, I. G. Stará, I. Starý, L. Rulíšek, D. Šaman, I. Císařová, *J. Org. Chem.* 2008, **73**, 2074-2082; c) J. Storch, J. Sýkora, J. Čermák, J. Karban, I. Císařová, A. Růžička, *J. Org. Chem.* 2009, **74**, 3090-3093.
25. Enantiomeric excess can be increased by more extensive purification but at the expense of yield (Scheme 1).
26. CCDC 718269 (**1**) and 718270 (**2**) contain the supplementary crystallographic data for this paper. These data can be obtained from The Cambridge Crystallographic Data Centre via http://www.ccdc.cam.ac.uk/data_request/cif
27. Computations studies: The ground state geometries for **2 a**, **3 a**, **5** were fully optimized within the C_2 point group of symmetry at the B3LYP/6-31G(d) level of theory and were determined to be at the minima by the vibrational analyses, using Gaussian 03 program (Ref: [29]). Analogous methods were used for **2 a**-*PM*, and employing the B3LYP/6-31G(d,p) level of theory, for model oligomers of [7]helicenes. Computational details can be found in the Supporting Information.
28. The computed geometry for **2 a** is similar to that determined by the X-ray crystallography for **2**.
29. Gaussian 03, Revision E.01, M. J. Frisch et al., Gaussian, Wallingford, CT, **2004**.
30. Phenylene-based 2,2′-bis[6]helicenes: a) W. H. Laarhoven, R. G. M. Veldhuis, *Tetrahedron* 1972, **28**, 1823-1827. The 2,2′-linkage between the [6]helicene units may be viewed as analogous to the α,α-linkage between carbon-sulfur [7]helicene units; nonracemic derivative of phenylene-based 2,2′-bis[5]helicene; b) S. D. Dreher, T. J. Katz, K.-C. Lam, A. L. Rheingold, *J. Org. Chem.* 2000, **65**, 815-822.

Supporting Information

Noncovalent Interactions in Asymmetric Synthesis of Rigid Conjugated Helical Structures

Makoto Miyasaka,[1†] *Maren Pink,*[2] *Suchada Rajca,*[1] *Andrzej Rajca*[1*]

[1]Department of Chemistry, University of Nebraska, Lincoln, Nebraska 68588-0304, USA.

[2]IUMSC, Department of Chemistry, Indiana University, Bloomington, Indiana 47405-7102, USA.

[*]To whom correspondence should be addressed. E-mail: arajca1@unl.edu.

[†]Current address: Department of Material and Life Chemistry, Faculty of Engineering, Kanagawa University, Yokohama 221-8686, Japan.

Table of Contents

1. Experimental Section.

1.a Materials and general procedures.

1.b X-ray crystallography (Figures S1–S3, and Table S1).

1.c UV-vis absorption spectroscopy, CD spectroscopy, and optical rotation (Figures S4–S6).

1.d Chiral HPLC and ^{1}H NMR spectroscopy with chiral shift reagents (Tables S2 and S3, Figures S7–S18).

1.e Synthesis of bis[7]helicene **2**, its attempted isomerization and annelation (Figures S19–S32).

1.f DFT calculations (Tables S4 and S5).

2. Supporting Text

3. Supporting Figures

4. Supporting Tables

5. Supporting References

1. Experimental Section.

1.a Materials and general procedures.

Ether and tetrahydrofuran (THF) for use on the vacuum line were freshly distilled from sodium/benzophenone prior to use; toluene was freshly distilled from sodium. For small-scale reactions, solvents were vacuum-transferred to volume-calibrated Schlenk vessels, immediately prior to the reaction. *t*-BuLi (pentane) and *n*-BuLi (hexane) were obtained from either Aldrich or Acros; prior to use, their concentrations were determined by titration with *N*-pivaloyl-*o*-toluidine.[S1] All other commercially available chemicals, including MeOD (99.5+ %D), were obtained from Aldrich, unless indicated otherwise. Column chromatography was carried out on TLC grade silica gel (Aldrich), using 0–20 psig pressure. Preparative TLC (PTLC) was carried out using Analtech silica plates (tapered with a preadsorbent zone). For purification of bis[7]helicene **2**, silica gel for column and thin layer chromatography were deactivated with 2–5% triethylamine in pentane. Standard techniques for synthesis under inert atmosphere, using Schlenk glassware and gloveboxes (Mbraun and Vacuum Atmospheres), were employed.

NMR spectra were obtained using Bruker spectrometers (^{1}H, 500 MHz and 400 MHz), using chloroform-*d*, benzene-d_6, toluene-d_8, or *p*-xylene-d_{10} as solvents. Most of the 500-MHz spectra were obtained using cryoprobe. The chemical shift references were as followings: ^{1}H, chloroform-*d*, (7.260 ppm, $CHCl_3$), benzene-d_6, (7.160 ppm, C_6D_5H), toluene-d_8 (2.090 ppm, $CD_2HC_6D_5$), and *p*-xylene-d_{10} (2.296 ppm, $CD_2HC_4D_4CD_3$), ^{13}C, chloroform-*d*, 77.00 ppm ($CDCl_3$). Typical 1D FID was subjected to exponential multiplication with an exponent of 0.1 Hz (for ^{1}H) and 1.0–2.0 Hz (for ^{13}C). Selected spectra were resolution enhanced, using exponential (LB, "line broadening") and Gaussian (GB, "Gaussian broadening") multiplications, with the values of the corresponding exponents, LB and GB, provided in Hz.

IR spectra were obtained using a Nicolet Avatar 360 FT-IR instrument, equipped with an ATR sampling accessory (Spectra Tech, Inc.). Compound (as solid or as solution in CH_2Cl_2) was applied to

the surface of a ZnSe ATR plate horizontal parallelogram (45°, Wilmad). After the solvent evaporated, the spectrum was acquired (128 scans, 4-cm^{-1} or 2-cm^{-1} resolution).

MS analyses were carried out at the Nebraska Center for Mass Spectrometry.

1.b X-ray crystallography (Figures S1–S3, and Table S1).

Single crystals for the X-ray crystallographic studies were obtained by slow evaporation of solvent at room temperature from solutions of tetrakis(β-trithiophene) **1** (benzene, sample label: MM-19-71-solid-cr1) and bis[7]helicene **2** (benzene/isopropanol (2:1), sample label: MM-21-04-TP1).

Data collection, structure solution, and refinement are briefly summarized below; more detailed description may be found in the crystallographic information files (CIFs).

Data collection, structure solution and refinement. Data for tetrakis(β-trithiophene) **1** and bis[7]helicene **2** were collected at the Advanced Photon Source, Argonne National Laboratory in Chicago, using synchrotron radiation (diamond 1 1 1 monochromators, two mirrors to exclude higher harmonics). For **1**, a wavelength of $\lambda = 0.43321$ Å, with a frame time of 2 s and a detector distance of 6.5 cm were used. For bis[7]helicene **2**, a wavelength of $\lambda = 0.48595$ Å, with a frame time of 1 s and a detector distance of 6.0 cm were used.

Single crystals were placed onto the tip of an ultra thin glass fiber. The intensity data were corrected for absorption[S2] for bis[7]helicene **2** and used uncorrected for **1**. Final cell constants were calculated from the xyz centroids of strong reflections from the actual data collection after integration.[S3]

Space groups were determined based on intensity statistics and systematic absences. Structures were solved with direct methods using Sir2004[S4] and refined with full-matrix least squares / difference Fourier cycles using SHELXL-97.[S5] All non-hydrogen atoms were refined with anisotropic displacement parameters. The hydrogen atoms were placed in ideal positions and refined as riding atoms with relative isotropic displacement parameters.

Tetrakis(β-trithiophene) 1. The compound crystallized in the space group C2/c with half of the molecule in the asymmetric unit. The final full matrix least squares refinement converged to R1 = 0.0402 and wR2 = 0.1227 (F2, all data). Propyl groups of TPS are disordered over two positions (ratio of approximately 62:38) and were refined with a set of restraints and constraints. The remaining electron density was located near the bromine atom.

Bis[7]helicene 2. The compound crystallized in the chiral space group $C222_1$ with half of the molecule and half of a solvent molecule (benzene) in the asymmetric unit. The crystal of **2** was found to be merohedrally twinned with an enantiomer ratio in the crystal of 88:12. One of the propyl groups is disordered over two positions (50:50) and was refined with a set of restraints and constraints. The final full matrix least squares refinement converged to R1 = 0.0405 and wR2 = 0.1011 (F2, all data). The remaining electron density was located near the sulfur atoms on bonds.

1.c UV-vis absorption spectroscopy, CD spectroscopy, and optical rotation (Figures S4–S6).

UV-vis spectra were recorded on Shimadzu (UV-2401PC) spectrophotometer, using cyclohexane as solvent. The Lambert-Beer plots were obtained using several solutions with the concentration range exceeding an order of magnitude; for all compounds studied, linear plots were obtained ($R^2 > 0.999$).

CD spectra were obtained using Jasco J-810 spectropolarimeter, equipped with a Peltier temperature controller. Five solutions of bis[7]helicene **2** in cyclohexane were prepared, and immediately following the collection of UV-vis data for the Lambert-Beer plot ($R^2 = 1.000$), CD spectra were recorded in 1-mm pathlength cells.

Optical rotations were measured with Autopol III (Rudolph Research) at ambient temperature.

1.d Chiral HPLC and ^{1}H NMR spectroscopy with chiral shift reagents (Tables S1 and S2, Figures S7–S18).

Chiral HPLC determinations for tetrakis(β-trithiophene) **1** and bis[7]helicene **2** were carried out using ChiralPak AD-H column (250-mm long) with 1.0 mL/min flow rate of hexane/isopropanol (*i*-PrOH) or hexane, as summarized in Table S2. Racemic [7]helicene **5**[S6] and racemic carbon-sulfur [11]helicene[S7] were used as references.

The ^{1}H NMR spectrum for tetrakis(β-trithiophene) **1** or bis[7]helicene **2** in chloroform-*d* (0.4 – 0.5 mL) was first obtained; then silver(I) 6,6,7,7,8,8,8-heptafluoro-2,2-dimethyl-3,5-octanedionate (Ag(fod)) and ytterbium(III) [tris-3-(heptafluoropropylhydroxymethylene)-(+)-camphorate] (Yb(hfpc)) were added until baseline separation between the peaks corresponding to the enantiomers (in fast exchange with diastereomeric complexes) was attained as summarized in Table S3.

1.e Synthesis of bis[7]helicene 2, its attempted isomerization and annelation (Figures S19–S32).

Typical procedure for preparation of LDA in ether/hexane. *n*-BuLi (2.56 M in hexane, 0.3 mL, 0.77 mmol) was added to diisopropylamine (0.12 mL, 0.85 mmol) in ether (2 mL) at 0 °C ($[c]_{LDA}$ = 0.32 M). After 2 h at 0 °C, the solution of LDA was ready for immediate use, or alternatively, neat (–)-sparteine (1.5 equiv) was added to obtain LDA/(–)-sparteine mixture.

Monoprotection: bis(β-trithiophene) 4a.

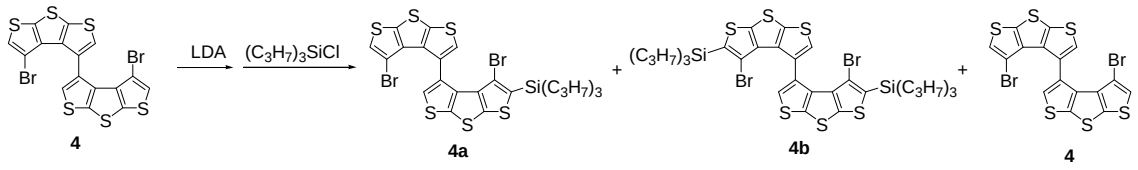

Summary for bis(β-trithiophene) **4a**.

Run	SM (mg)	Ether (mL)	LDA		$(n\text{-Pr})_3SiCl$[b] (equiv)	**4b** (mg, %)	**4a** (mg, %)	**4** (mg, %)
			(equiv)	Temp/Time (K)/(h)				
MM1298	100.0	35	1.1	273/6[a]	1.2	5.8, 4	55.1, 43	-
MM1306	56.8	35	1.5	273/6	1.8	13.8, 15	21.5, 29	3.0, 5
MM1817	100.0	35	1.5	273/6	1.8	29.3, 19	44.4, 34	22.4, 22
MM1918[c]	200.0	70	1.5	273/7	1.8	119, 19	154, 30	56.4, 14
MM1923	200.4	70	1.6	273/7.5	1.9			
MM1945[d]							27, 18 (35)	
MM1946	205.6	72	1.5	273/8.3	1.8			
	119.4	42	1.5	273/8.3	1.8	87, 17	103, 25	38, 12
MM1967[e]	50.8	18	1.5	273/7	1.8	Failed		
MM1976[e,f]	45.1	18	1.5	273/7	1.8	67.3, 18	128.4, 41	72.4, 30
MM1997[e,f]	200.4	80	1.5	273/7	1.8			
MM2012[e,f]	92.8	37	1.5	273/7	1.8	13.8, 10	41.6, 35 (170.0, 66)[g]	23.8, 26

[a] After 6 h at 273 K, the reaction mixture was warmed to room temperature, and then stirred for 1 h, prior to cooling to 273 K for the addition of $(n\text{-Pr})_3SiCl$.
[b] The addition of $(n\text{-Pr})_3SiCl$ was carried out at 273 K.
[c] This reaction crude mixture was combined with another crude (MM-19-23), and the combined crudes were purified by column chromatography.
[d] The side product **4b** from MM-19-23 was completely de-silylated, and then combined with the unreacted starting material **4**. The combined **4** was recycled with LDA and chlorotripropylsilane. The additional 27 mg of **4a** was obtained. The overall yield of **4a** was 35%.
[e] The solvent was toluene instead of ether.
[f] (–)-Sparteine (4 equiv vs. **4**) was added after addition of LDA.
[g] One recycle was carried out (MM-19-97, and then MM-20-12); total 179.0 mg (66%) of **4a** was obtained from 200.4 mg of **4**.

Bis(β-trithiophene) 4a, without recycling (MM-19-23). LDA in ether/hexane (0.32 M, 1.8 mL, 0.57 mmol, 1.6 equiv) was added by syringe to bis(4,4'-dibromodithieno[2,3-b:3',2'-d]thiophene) (**4**) (200.4

mg, 0.365 mmol, 1 equiv, MM-17-72-solid) in ether (70 mL) at 0 °C. The reaction mixture (brown yellow suspension) was stirred for 7.5 h at 0 °C, and then chlorotripropylsilane (0.15 mL, 0.685 mmol, 1.9 equiv) was added to reaction mixture at 0 °C. The reaction mixture was briefly kept at 0 °C, and then allowed to warm slowly to ambient temperature. After the reaction mixture was stirred for 1 – 2 days at ambient temperature, the usual aqueous extraction with benzene was carried out, to provide the crude product as brown oil (0.355 g). This crude product was combined with the crude product from other reactions on the 200-mg scale (MM-19-18), and purified by a column chromatography (silica, hexane/dichloromethane, 5:1), to give the three fractions: F1, bis(4,4'-dibromodithieno-5,5'-di(tripropylsilyl)-[2,3-b:3',2'-d]thiophene) (**4b**) (119 mg, 19%, R_f = 0.72); F2, bis(4,4'-dibromodithieno-5-tripropylsilyl-[2,3-b:3',2'-d]thiophene) (**4a**) (154.0 mg, 30%, R_f = 0.57); F3, bis(4,4'-dibromodithieno[2,3-b:3',2'-d]thiophene) (**4**) (56.4 mg, 14%, R_f = 0.45). From other five reactions on 100-, 50-, 100-, 200-, and 120-mg scales (MM-12-98, 13-06, 18-17, 19-46), 135.9 mg (4 – 19%) of **4b**, 224 mg (25 – 43%) of **4a**, and 63.4 mg (5 – 22%) of **4** were obtained from 581.8 g of **4** without recycling **4b** and **4**.

Bis(β-trithiophene) 4a, with recycling (MM-19-97, MM-19-76, MM-20-12). LDA in ether/hexane (0.32 M, 1.7 mL, 0.54 mmol, 1.5 equiv) was added by syringe to bis(4,4'-dibromodithieno[2,3-b:3',2'-d]thiophene) (**4**) (200.4 mg, 0.365 mmol, 1 equiv) in toluene (80 mL) at 0 °C. After 20 min at 0 °C, (–)-sparteine (0.34 mL, 1.46 mmol, 4 equiv) was added to the reaction mixture. The reaction mixture (brown yellow suspension) was stirred for 7 h at 0 °C, and then chlorotripropylsilane (0.14 mL, 0.658 mmol, 1.8 equiv) was added to reaction mixture at 0 °C. The reaction mixture was briefly kept at 0 °C, and then allowed to warm slowly to ambient temperature. Subsequently, the reaction mixture was typically kept stirring for 1 – 2 days at ambient temperature. The usual aqueous extraction with benzene gave the crude product as brown oil. This crude product was combined with the crude product from another reaction on the 45-mg scale (MM-19-76), and purified by a column chromatography (silica, hexane/dichloromethane, 5:1). After the purification,

128.4 mg (41%) of **4a** was obtained from 245.5 mg of **4**. The side product **4b** (67.3 mg, 18%) was converted to **4** using trifluoracetic acid in chloroform (MM-20-11), and then combined with unreacted **4** (72.4 mg, 30%). The combined **4** was treated with LDA and chlorotripropylsilane, as described above. The additional 41.6 mg (35%) of **4a** was obtained from 92.8 mg of **4** (MM-20-12). The overall yield of **4a** was 170 mg (66%) after one recycle.

Bis(4,4'-dibromodithieno-5-tripropylsilyl-[2,3-b:3',2'-d]thiophene: bis(β-trithiophene) 4a. M.p. 50 – 51 °C (powder becomes a bulk solid), 57 – 58 °C (changed to clear jelly-like solid). ^{1}H NMR (400 MHz, $CDCl_3$): δ = 7.364 (s, 1 H), 7.340 (s, 1 H), 7.083 (s, 1 H), 1.36 – 1.22 (m, 6 H), 0.888 (t, *J* = 7.2, 9 H), 0.85 – 0.77 (m, 6 H). ^{13}C{^{1}H} NMR (100 MHz, $CDCl_3$): δ = aromatic region, expected 16 resonances; found 16 resonances at 143.8, 140.3, 139.9, 139.7, 139.2, 138.9, 138.3, 137.2, 135.6, 130.6, 130.2, 127.72, 127.69, 124.3, 109.0, 102.4, aliphatic region, expected 3 resonances; found 3 resonances at 18.3, 17.3, 15.1. IR (cm^{-1}): 3102, 2952, 2922, 2864 (C-H). LR/HR FABMS (3-NBA matrix): *m/z* (ion type, % RA for *m/z* = 650 – 1000, deviation for the formula): 701.8333 ($[M]^+$, 51 %, 0.7 ppm for $^{12}C_{25}{}^{1}H_{24}{}^{28}Si_1{}^{32}S_6{}^{79}Br_2$), 702.8378 ($[M+1]^+$, 41 %, –0.8 ppm for $^{12}C_{24}{}^{13}C_1{}^{1}H_{24}{}^{28}Si_1{}^{32}S_6{}^{79}Br_2$), 703.8327 ($[M+2]^+$, 99 %, –1.2 ppm for $^{12}C_{25}{}^{1}H_{24}{}^{28}Si_1{}^{32}S_6{}^{79}Br_1{}^{81}Br_1$), 705.8315 ($[M+4]^+$, 96 %, –2.6 ppm for $^{12}C_{25}{}^{1}H_{24}{}^{28}Si_1{}^{32}S_6{}^{81}Br_2$), 706.8320 ($[M+5]^+$, 73 %, 1.6 ppm for $^{12}C_{24}{}^{13}C_1{}^{1}H_{24}{}^{28}Si_1{}^{32}S_6{}^{81}Br_2$).

Bis(4,4'-dibromodithieno-5,5'-di(tripropylsilyl)-[2,3-b:3',2'-d]thiophene): bis(β-trithiophene) 4b. Soft solid at room temperature. ^{1}H NMR (400 MHz, $CDCl_3$): δ = 7.336 (s, 2 H), 1.33 – 1.19 (m, 12 H), 0.882 (t, *J* = 7.2, 18 H), 0.84 – 0.77 (m, 12 H). ^{13}C{^{1}H} NMR (100 MHz, $CDCl_3$): δ = aromatic region, expected 8 resonances; found 8 resonances at 143.8, 140.3, 139.7, 138.5, 135.3, 130.8, 127.4, 109.1, aliphatic region, expected 3 resonances; found 3 resonances at 18.3, 17.3, 15.1. IR (cm^{-1}): 3099, 2953, 2923, 2866 (C-H). LR/HR FABMS (3-NBA matrix): *m/z* (ion type, % RA for *m/z* = 700 – 1000, deviation for the formula): 857.9686 ($[M]^+$, 37 %, –1.6 ppm for $^{12}C_{34}{}^{1}H_{44}{}^{28}Si_2{}^{32}S_6{}^{79}Br_2$), 859.9622 ($[M+2]^+$, 99 %, 3.6 ppm for $^{12}C_{34}{}^{1}H_{44}{}^{28}Si_2{}^{32}S_6{}^{79}Br_1{}^{81}Br_1$), 861.9640 ($[M+4]^+$, 100 %, –0.9 ppm for $^{12}C_{34}{}^{1}H_{44}{}^{28}Si_2{}^{32}S_6{}^{81}Br_2$), 862.9667 ($[M+5]^+$, 81 %, –0.3 ppm for $^{12}C_{33}{}^{13}C_1{}^{1}H_{44}{}^{28}Si_2{}^{32}S_6{}^{81}Br_2$). UV/vis,

cyclohexane, λ_{max}/nm (ε_{max}/L mol^{-1} cm^{-1}) (MM-21-11): 265 (3.63 × 10^4), 227 (6.28 × 10^4), 203 (3.63 × 10^4).

Connection: tetrakis(β-trithiophene) 1.

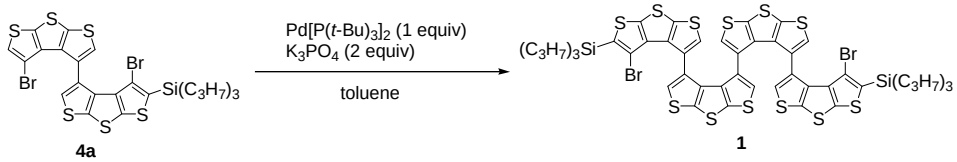

Summary for tetrakis(β-trithiophene) **1**.

Run	SM (mg)	TM (mg, %)
MM1426	2.8	1.0, 40
MM1429	10.2	3.6, 40
MM1572	16.9	6.9, 46
MM1826[a]	11.0	12.3, 26
MM1829	42.0	
MM1925[b]	50.5	29.6, 33
MM1928	51.0	
MM1971	50.9 51.9	31.1, 34
MM2112	76.6 75.0	45.2, 34

[a] This crude was combined with MM1829 and purified.
[b] This crude was combined with MM1928 and purified.

Tetrakis(β-trithiophene) 1 (MM-19-28). Bis(β-trithiophene) **4a** (51 mg, 72.4 μmol, 1.0 equiv), K_3PO_4 (37.3 mg, 0.176 mmol, 2.4 equiv) and Pd(P(*t*-Bu)$_3$)$_2$ (38.3 mg, 74.9 μmol, 1.03 equiv) in toluene (6 mL) were stirred at 90 °C in a Schlenk vessel overnight. The usual aqueous workup with ether gave the crude product as a brown solid. This crude product was combined with the crude products from another reaction on the 50-mg scale (MM-19-25), and purified by a column chromatography (silica, hexane/chloroform, 3:1, R_f = 0.78) and PTLC (silica, hexane/chloroform, 3:1) to provide tetrakis(β-trithiophene) **1** (29.6 mg, 33%) from 101.5 mg of **4a**. M.p. 309–310 °C. ^{1}H NMR (400 MHz, $CDCl_3$): δ = 7.046 (s, 2 H), 6.707 (s, 2 H), 6.241 (s, 2 H), 1.38 – 1.19 (m, 12 H), 0.882 (t, *J* = 7.2, 18 H), 0.87 – 0.76 (m 12 H). ^{13}C{^{1}H} NMR (100 MHz, $CDCl_3$): δ = aromatic region, expected 16 resonances; found 16 resonances at 143.7, 140.4, 140.1, 139.9, 138.4, 138.0, 137.4, 135.6, 135.0, 130.5, 128.2, 128.0, 127.4, 127.24, 127.21, 109.1, aliphatic region, expected 3 resonances; found 3 resonances

at 18.2, 17.4, 15.0. IR (cm^{-1}): 3097, 2953, 2924, 2866 (C-H). LR/HR FABMS (3-NBA matrix): *m/z* (ion type, % RA for *m/z* = 1000 – 1500, deviation for the formula): 1245.8292 ($[M]^+$, 31 %, 1.5 ppm for $^{12}C_{50}{}^{1}H_{48}{}^{28}Si_2{}^{32}S_{12}{}^{79}Br_2$), 1246.8332 ($[M+1]^+$, 31 %, 0.9 ppm for $^{12}C_{49}{}^{13}C_1{}^{1}H_{48}{}^{28}Si_2{}^{32}S_{12}{}^{79}Br_2$), 1247.8285 ($[M+2]^+$, 91 %, 0.3 ppm for $^{12}C_{50}{}^{1}H_{48}{}^{28}Si_2{}^{32}S_{12}{}^{79}Br_1{}^{81}Br_1$), 1248.8296 ($[M+3]^+$, 81 %, 2.2 ppm for $^{12}C_{49}{}^{13}C_1{}^{1}H_{48}{}^{28}Si_2{}^{32}S_{12}{}^{79}Br_1{}^{81}Br_1$), 1249.8275 ($[M+4]^+$, 100 %, –0.4 ppm for $^{12}C_{50}{}^{1}H_{48}{}^{28}Si_2{}^{32}S_{12}{}^{81}Br_2$). UV/vis, cyclohexane, λ_{max}/nm (ε_{max}/L mol^{-1} cm^{-1}) (MM-21-09): 266 (shoulder, 4.40×10^4), 225 (9.20×10^4). ^{1}H NMR spectrum with chiral shift reagents: ^{1}H NMR (500 MHz, LB = –0.8 Hz, GB = 0.3 Hz, tetrakis(β-trithiophene) **1** (0.8 mg), Ag(fod) (2.2 mg), and Yb(hfpc) (2.7 mg)): δ = aromatic region, 7.074 (s, 1 H), 7.054 (s, 1H), 6.726 (s, 1H), 6.721 (s, 1 H), 6.242 (s, 1 H), 6.233 (s, 1 H), aliphatic region, 0.883 (t, *J* = 7.5, 3 H), 0.879 (t, *J* = 7.5, 3 H).

Double ring annelation: bis[7]helicene 2.

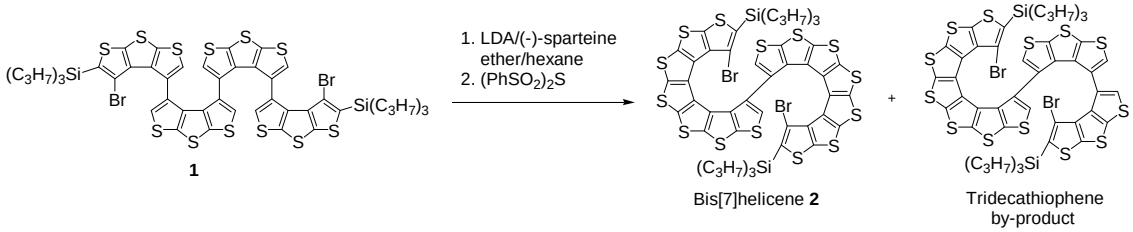

Summary of synthesis of bis[7]helicene **2**.

Label	SM/ether	LDA	Addition of LDA	$(PhSO_2)_2S$/ether		Bis[7]helicene **2**		
	(mg/mL)	equiv[a]	temp (K)/time (min)	mg/mL	equiv	(mg, %)	NMR (ee %)	HPLC[c] (ee %)
MM1446	2.5/1.2	12	273/120, 295-6/120, 273/30	3.0/0.8	4.8	1.3, 50		
MM1588	3.4/2.2	12	273/120, 295/120, 273/30	3.8/0.8	4.4	1.4, 39		
MM1859	3.0/1.8	12	273/120, 298-9/180, 273/30	10.5/1.7	6.0	0.7, 23		47
MM1948[b]	6.4/4.0	12	273/120, 298/180, 273/30	12.3/2.2	6.0	2.3, 13	7.8[d]	25[d]
MM1953	10.0/6.4	12	273/120, 298/180, 273/30	17.6/2.9	6.0			
MM1957	9.5/6.0	12	273/120, 298/180, 273/30	16.9/2	6.0	1.4, 14	7.8[e]	21
MM1989	4.0/2.4	18	273/120, 306/180, 273/30	15.8/1.8	10	0.4, 9.5		
MM2115	29.4/20	12.8	273/120, 298/180, 273/30	45.8/5	10	1.1, 3.6		62
MM2126	30.0/20	12.5	273/120, 298/180, 273/30	54.5/5	10	1.1, 3.5 2.7, 8.6		68 5

[a] LDA/(−)-sparteine, 1:1.5
[b] This crude mixture was combined with MM-19-53 and purified.
[c] The mobile phase was hexane (1 mL/min flow rate).
[d] This sample preparation may not be homogeneous.
[e] Homogeneous sample.

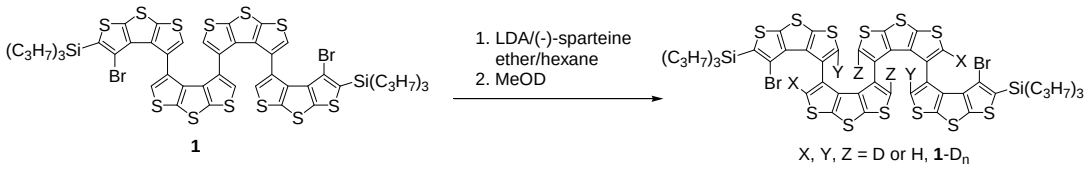

Summary of MeOD-quenching experiments.

Label	SM/ ether	LDA	Addition of LDA	^{1}H NMR relative integrations for deuterated **1** (CH_2 and CH_3 groups set to 15H)		
	(mg/mL)	equiv[a]	temp (K)/time (min)	6.230 ppm	6.703 ppm	7.045 ppm
MM1871	2.5/1.2	12	273/120, 298/180, 195/30	0.67	0.16	0.05
MM1884	1.5/0.8	18	273/120, 308-9/180, 195/30	0.34	0.17	0.07
MM1892	1.3/0.2	~400	273/120, 298-9/180, 195/10	0.34	0.02	0.04
MM1906	1.3/0.7	30	273/120, 313/880, 195/30	0.53	0.07	0.06

[a] LDA/(−)-sparteine, 1:1.5.

Bis[7]helicene 2 (MM-21-26). The LDA/(–)-sparteine solution (0.28 M in ether/hexane, 1.00 mL, 0.28 mmol, 12 equiv of LDA, with LDA/(–)-sparteine, 1:1.5) was added to tetrakis(β-trithiophene) **1** (30.0 mg, 24.0 μmol, 1.0 equiv) in ether (20 mL) at 0 °C. After 2 h at 0 °C, the reaction mixture (white suspension) was allowed to attain room temperature (~298 K), and then kept stirring for another 3 h; the reaction mixture became more homogeneous and pale yellow. The ether solution of bis(phenylsulfonyl)sulfide (54.5 mg/5 mL) (4.2 mL, 0.144 mmol, 6 equiv) was added to the reaction mixture at 0 °C. The reaction mixture was allowed to attain ambient temperature (pale yellow suspension) over 12 h. The usual aqueous workup with ether and benzene gave the crude product as a pale brown solid (52.2 mg); using the solution of the crude product, a small sample was put aside for analytical measurements. Purification was carried out by multiple PTLC separations using deactivated silica (3% triethylamine in pentane); the PTLC plates were developed either in cold room or at room temperature, using heptane/benzene (6:1) and/or 5% ethyl acetate in heptanes. The final PTLC (deactivated silica, 5% ethyl acetate in heptanes, room temperature) gave bis[7]helicene **2** (1.1 mg, 3.5 %, ee 68 %) as a pale yellow solid. Due to low solubility of **2** and tailing on silica, most of the remaining PTLC plate was eluted, and the resultant solid was treated with pentane and methanol, to provide a second fraction of nearly racemic bis[7]helicene **2** (2.7 mg, 8.6%, ee ~5%) as a white solid. Thus, overall yield was 3.8 mg, ~12%.

From another reaction (MM-15-88) on the 3.4-mg scale, 1.4 mg (39%) of bis[7]helicene was obtained as the least polar fraction (MM-15-88-TP1) after single PTLC (silica, hexane/benzene, 6:1) purification. The fraction obtained by elution of the remaining silica plate (2.8 mg, MM-15-88-TP3) was separated by analytical TLC (silica, hexane/benzene, 6:1), to provide two fractions (0.3 mg and 0.2 mg), both containing a mixture of bis[7]helicene **2** and tridecathiophene by-product based upon LR FABMS data. ^{1}H NMR spectrum and LR FABMS for the fraction with lower R_f (0.2 mg, MM-15-88-TP3B) are shown in Figures S25 and S26, respectively.

Bis[7]helicene 2. The sample used for the melting point determination was nearly racemic (ee ~5%, label: MM-21-26-TP2+TP3-A-4+5-solid). M.p. (dec., under air): 315–318 °C (pale brown solid).

M.p. (dec., under argon): ~370 °C (pale brown solid). ^{1}H NMR (400 MHz, $CDCl_3$): δ = 7.024 (s, 2 H), 1.43 – 1.28 (m, 12 H), 0.947 (t, *J* = 7.2, 18 H), 0.92 – 0.77 (m, 12 H). ^{1}H NMR (500 MHz, benzene-d_6, MM-19-57-TP2-benzene2): δ = 7.292 (s, 2 H), 1.44 – 1.30 (m, 12 H), 1.012 (t, *J* = 7.0, 18 H), 0.93 – 0.77 (m, 12 H). ^{1}H NMR (500 MHz, toluene-d_8, MM-20-25-2): δ = 7.243 (s, 2 H), 1.44 – 1.30 (m, 12 H), 1.018 (t, *J* = 7.0, 18 H), 0.93 – 0.79 (m, 12 H). ^{13}C{^{1}H} NMR (100 MHz, $CDCl_3$): δ = aromatic region, expected 16 resonances; found 16 resonances at 143.2, 140.1, 139.7, 139.5, 137.42, 137.36, 136.84, 136.81, 132.1, 131.9, 130.3, 130.0, 128.73, 128.70, 126.8, 111.9, aliphatic region, expected 3 resonances; found 3 resonances at 18.5, 17.5, 15.3. IR (cm^{-1}): 3112 (very weak), 2952, 2922, 2865 (C-H). LR/HR FABMS (3-NBA matrix): *m/z* (ion type, % RA for *m/z* = 800 – 1600, deviation for the formula): 1305.7400 ($[M]^+$, 30 %, 2.9 ppm for $^{12}C_{50}{}^{1}H_{44}{}^{28}Si_2{}^{32}S_{14}{}^{79}Br_2$), 1306.7434 ($[M+1]^+$, 28 %, 2.9 ppm for $^{12}C_{49}{}^{13}C_1{}^{1}H_{44}{}^{28}Si_2{}^{32}S_{14}{}^{79}Br_2$), 1307.7372 ($[M+2]^+$, 84 %, 3.5 ppm for $^{12}C_{50}{}^{1}H_{44}{}^{28}Si_2{}^{32}S_{14}{}^{79}Br_1{}^{81}Br_1$), 1308.7409 ($[M+3]^+$, 70 %, 3.3 ppm for $^{12}C_{49}{}^{13}C_1{}^{1}H_{44}{}^{28}Si_2{}^{32}S_{14}{}^{79}Br_1{}^{81}Br_1$), 1309.7375 ($[M+4]^+$, 100 %, 1.7 ppm for $^{12}C_{50}{}^{1}H_{44}{}^{28}Si_2{}^{32}S_{14}{}^{81}Br_2$), 1310.7384 ($[M+5]^+$, 69 %, 3.6 ppm for $^{12}C_{49}{}^{13}C_1{}^{1}H_{44}{}^{28}Si_2{}^{32}S_{14}{}^{81}Br_2$). ^{1}H NMR spectrum with chiral shift reagents: ^{1}H NMR (500 MHz, $CDCl_3$, LB = –0.8 Hz, GB = 0.4 Hz, bis[7]helicene **2**-$(TPS)_2$ (0.4 mg), Ag(fod) (3.0 mg), and Yb(hfpc) (2.8 mg)): δ = aromatic region, 7.070 (s, 1.00 H), 7.060 (s, 1.17 H).

Chirooptical data for bis[7]helicene 2. HPLC, ee 62%. UV/vis (MM-21-41), cyclohexane, λ_{max}/nm (ε_{max}/L mol^{-1} cm^{-1}) (MM-21-09): 258 (4.40×10^4), 242 (5.83×10^4), 217 (5.58×10^4), 204 (6.10×10^4). $[\alpha]_D^{rt}$ = –756 (*c* = 5.8×10^{-5}, cyclohexane). CD (MM-21-41-CD100), cyclohexane, λ_{max}/nm ($\Delta\varepsilon_{max}$/L mol^{-1} cm^{-1}): 284 (–115), 255 (21), 231 (–101), 216 (20), 205 (–19), 196 (21).

Tridecathiophene by-product. ^{1}H NMR (500 MHz, $CDCl_3$, Figure S24): δ = 6.804 (s, 1 H), 6.758 (s, 1 H), 6.333 (s, 1 H), 6.085 (s, 1 H), 1.4 – 1.3 (m, 12H), 1.0 – 0.8 (m, 30 H). LR FABMS (3-NBA matrix): Figure S25, HR FABMS (3-NBA matrix): *m/z* (ion type, % RA for *m/z* = 1275 – 1282, deviation for the formula): 1275.7910 ($[M]^+$, 27 %, –2.8 ppm for $^{12}C_{50}{}^{1}H_{46}{}^{28}Si_2{}^{32}S_{13}{}^{79}Br_2$), 1276.7918 ($[M+1]^+$, 36 %, –0.8 ppm for $^{12}C_{49}{}^{13}C_1{}^{1}H_{46}{}^{28}Si_2{}^{32}S_{13}{}^{79}Br_2$), 1277.7838 ($[M+2]^+$, 83 %, 1.2 ppm for

$^{12}C_{50}{}^{1}H_{46}{}^{28}Si_2{}^{32}S_{13}{}^{79}Br_1{}^{81}Br_1$), 1278.7883 ([M+3]$^+$, 83 %, 0.3 ppm for $^{12}C_{49}{}^{13}C_1{}^{1}H_{46}{}^{28}Si_2{}^{32}S_{13}{}^{79}Br_1{}^{81}Br_1$), 1279.7865 ([M+4]$^+$, 100 %, –2.5 ppm for $^{12}C_{50}{}^{1}H_{46}{}^{28}Si_2{}^{32}S_{13}{}^{81}Br_2$), 1280.7880 ([M+5]$^+$, 83 %, –1.0 ppm for $^{12}C_{49}{}^{13}C_1{}^{1}H_{46}{}^{28}Si_2{}^{32}S_{13}{}^{81}Br_2$).

Attempted isomerization of bis[7]helicene 2.

The isomerization experiments are summarized in the Supporting Text Section and in the Supporting Figures Section (Figures S30–S32).

Attempted annelation of bis[7]helicene 2.

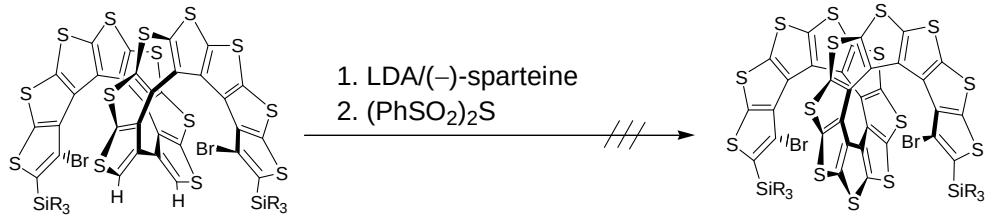

R = $CH_3CH_2CH_2$, **2**
bis[7]helicene

R = $CH_3CH_2CH_2$, **3**
[15]helicene

Summary of attempted annelation of bis[7]helicene to [15]helicene.

Label	SM (mg)	LDA/(-)sparteine (equiv)	Addition of LDA/(-)sparteine	Solvent	$(PhSO_2)_2S$ (equiv)	Comment
MM-19-61	1.7	4-5	0 °C, then 3 h at rt	ether	3.5	Suspension at all times; only SM recovered
MM-19-64	1.1	4-5	0 °C, then 3 h at rt	toluene	5	LR-FABMS (ONPOE): *m/z* 1309.6 (strong) and 1340.7 (v. weak).
MM-19-87	1.0	5	0 °C, then 3 h at 308 K	ether	5	LR-FABMS (ONPOE): *m/z* 1309.6 (strong) and nothing at higher *m/z*.

1.f DFT calculations (Tables S4 and S5).

All calculations were performed at 298 K by the Gaussian03 program package running on an 8-cpu workstation under Linux operating system.[S8]

Ground-state geometries were optimized at the B3LYP/6-31G(d) level within the two-fold symmetric point group (C_2 or C_i). Vibrational analyses were carried out to confirm the minima corresponding to the C_2-symmetric structures for bis[7]helicene **2a**, [15]helicene **3a**, and [7]helicene **5** (*MM*- or *M*-enantiomers). C_i-symmetric structure for bis[7]helicene **2a**-*PM* was found to be a transition state but with a very small imaginary frequency (i2 cm^{-1}), indicating a very flat potential energy surface; full geometry optimization (C_1 point group) and subsequent vibrational analysis gave minimum on the potential energy surface with very small lowest vibrational frequency of about 5 cm^{-1} and with practically identical total energy to that of the C_i-symmetric transition state, thus suggesting that the structure is fluxional with respect to twisting about the helicene-helicene linkage. (The energy of the C_1-symmetric structure was somewhat higher energy after the ZPE correction.)

Analogously, the ground state geometries within C_2 or C_i point group were optimized at the B3LYP/6-31G(d,p) level for model bis-, tris-, tetrakis-[7]helicenes that correspond to the diastereomers in which all helicene-helicene linkages between the β-positions of the terminal thiophenes (β,β-linkages) are either of the same chirality or of the opposite chirality. Similar geometry optimizations were carried out for the corresponding model bis[7]helicenes in which the helicene-helicene linkages were between the α-positions of the terminal thiophenes (α,α-linkages). All optimized geometries have RMS forces in Cartesian coordinates less than 2×10^{-6} a.u. (and about one order of magnitude lower in internal coordinates), i.e., significantly better than the "tight" criterion for RMS forces in geometry optimization in Gaussian03. Vibrational analyses were carried out for all bis[7]helicenes, tris[7]helicenes, and tetrakis[7]helicenes to confirm the corresponding minima; the exception was the C_i-symmetric structure for bis[7]helicene **9**-*PM* (Table S5) with the α,α-linkage, which possessed one small imaginary frequency (i5 cm^{-1}). The potential energy surfaces were rather flat, especially for the oligomers of [7]helicenes with

the linkages of opposite chirality. The ZPE corrections to energy were not scaled by the usual scaling factor of 0.9806 for the B3LYP/6-31(d) method;[S9,S10] the differences between the relevant ZPE's were very small, so such scaling would have negligible impact on the relative energies. (Similar considerations apply to the ZPE's and relative energies obtained by the B3LYP/6-31G(d,p) method.) The key results for the optimized structures and their vibrational analyzes are summarized in Tables S4 and S5.

Using the C_2- and C_i-symmetric gas phase geometries, the time-dependent density functional response theory (TDDFT) calculations at the B3LYP/6-31G(d) and B3LYP/6-31+G(d) levels of theory provided excitation energies and rotatory strength R in the dipole velocity form (R_{vel}) and dipole length form (R_{len}) for electronic circular dichroism (CD) spectra for bis[7]helicene **2a**, [15]helicene **3a**, and [7]helicene **5** (*MM*- or *M*-enantiomers). In addition, TDDFT calculations at the B3LYP/6-31G(d) level of theory for bis[7]helicene **2** (*MM*-enantiomer) were carried out using its X-ray structure geometry (C_1 point group). For all studied compounds, the values of R_{vel} and R_{len} were practically indistinguishable.

The inclusion of solvent models for cyclohexane such as integral equation formalism of the polarizable continuum model (IEF-PCM) were found to be essential for adequate reproduction of the long-wavelength part of the CD spectrum for bis[7]helicene. PCM is expected to be a valid approximation of solvent effects because no specific interactions (such as hydrogen bonds, ion pairing) link the solute and the cyclohexane solvent molecules. Different schemes for assigning atomic radii (UA0, UAHF, and Bondi) in the Gaussian03 were considered;[S11,S12] our TD-B3LYP calculations on [7]helicene **5** suggested that the performance of these schemes is similar, with slightly better fit between the calculated and experimental CD spectra for the united-atom Hartree-Fock (UAHF) radii. Inclusion of the diffuse functions in the basis set (6-31+G(d)) led to a greater red-shift for the calculated CD spectra for both [7]helicene **5** and bis[7]helicene **2a**. Therefore, the final CD spectra were calculated at the TD-B3LYP level with the 6-31G(d) basis set and with the IEF-PCM-UAHF solvent model for cyclohexane, and using the B3LYP/6-31G(d) gas-phase optimized geometries; also, these calculations provided electronic absorption spectra for bis[7]helicene **2a**, [15]helicene **3a**, and [7]helicene **5**, as well as for C_i-symmetric bis[7]helicene

2a-*PM*. In the final TD-B3LYP calculations, 210 and 190 excited states were calculated for [15]helicene **3a** and bis[7]helicene **2a**, respectively.

The electronic CD data (R_{len}) in the Gaussian03 output files were converted to stick spectra in the text file format and then convoluted with the Gaussian functions with half-width of 0.2 eV, using graphical user interface Gabedit (version 2.1.8, http://gabedit.sourceforge.net). The resultant spectra were re-plotted with the wavelength (nm) axis using SigmaPlot program. Analogous procedures were employed for extraction and plotting of the electronic absorption spectra.

For all calculated spectra, vertical axes were scaled to fit the experimental spectra. For bis[7]helicenes **2a** and **2a**-*PM*, and [15]helicene **3a**, the horizontal axes were not scaled; for [7]helicene **5**, the calculated spectra were blue-shifted by applying scaling factor of 1.035 to the transition energies (eV), prior to the conversion to the wavelength (nm).

2. Supporting Text

As indicated in note 25 (main text), enantiomeric excess (ee) can be increased by more extensive purification process but at the expense of yield (Scheme 1). For example, separation of bis[7]helicene **2** by preparative TLC (deactivated silica using 3% triethylamine in pentane, 5% ethyl acetate in heptanes as eluent, room temperature) gives a fraction with enriched ee of about 68% (Fig. S14, Table S2). Due to low solubility of **2**, the larger fraction of the bis[7]helicene is tailing on the preparative TLC plate, and it is nearly racemic (~5% ee) as shown in Fig. S15 (Table S2).

The identical configuration for all three β,β-linkages for tetrakis(β-trithiophene) **1** in the solid state is also indicated by the identical signs of the torsion angles (Table S1).

Crystal packing plots for both tetrakis(β-trithiophene) **1** and bis[7]helicene **2** show multiple short contacts but no significant π-stacking between the molecules (Fig. S2).

As a minor comment concerning conformations of both tetrakis(β-trithiophene) **1** and bis[7]helicene **2** in solution, we note that their ^{1}H NMR spectra suggest that the methylene groups in the TPS groups are diastereotopic, as expected for molecules that are chiral on the NMR time scale.

In the isomerization experiments for **2**, the bis[7]helicene was either heated in the solid state at 280 °C for 1 h under argon atmosphere or in *p*-xylene-d_{10} solution at 200 °C for 10 h (Figs. S30–S32). These conditions are limited by an onset of decomposition of **2**. Under similar conditions [7]helicene **5** racemizes; e.g., half-life for racemization in the solid state is 11±1 h at 199 °C or about 5 h at 203 °C.[S6]

In the attempted triple ring annelation of bis[7]helicene **2** to provide [15]helicene, FABMS analyses of crude reaction mixtures and of selected chromatographic fractions revealed weak ion clusters at *m/z* 1341–1342, in addition to a strong ion cluster at *m/z* 1309–1310 for **2**. For example, run MM1989, using the conditions for lithiation that are identical to those in the MeOD-quenching run MM1884 (p. S12). However, no conclusive evidence for [15]helicene was obtained.

3. Supporting Figures

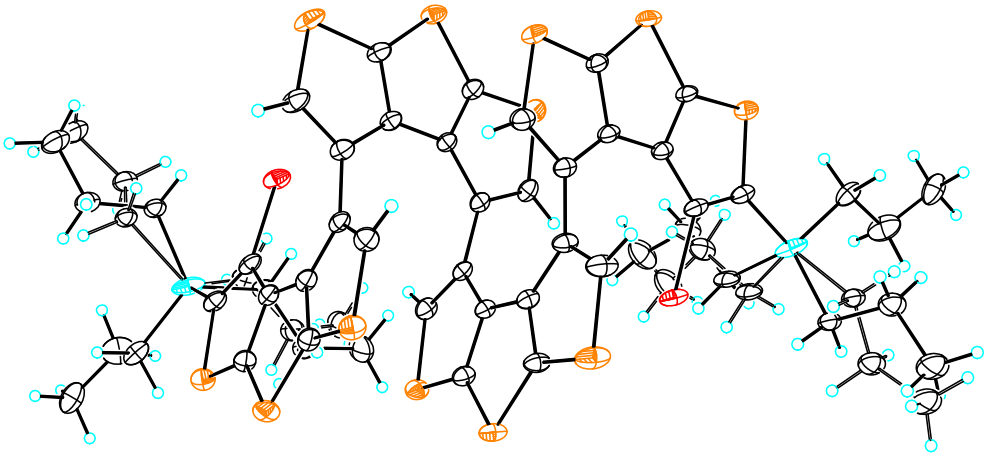

Formula unit, disorder shown.

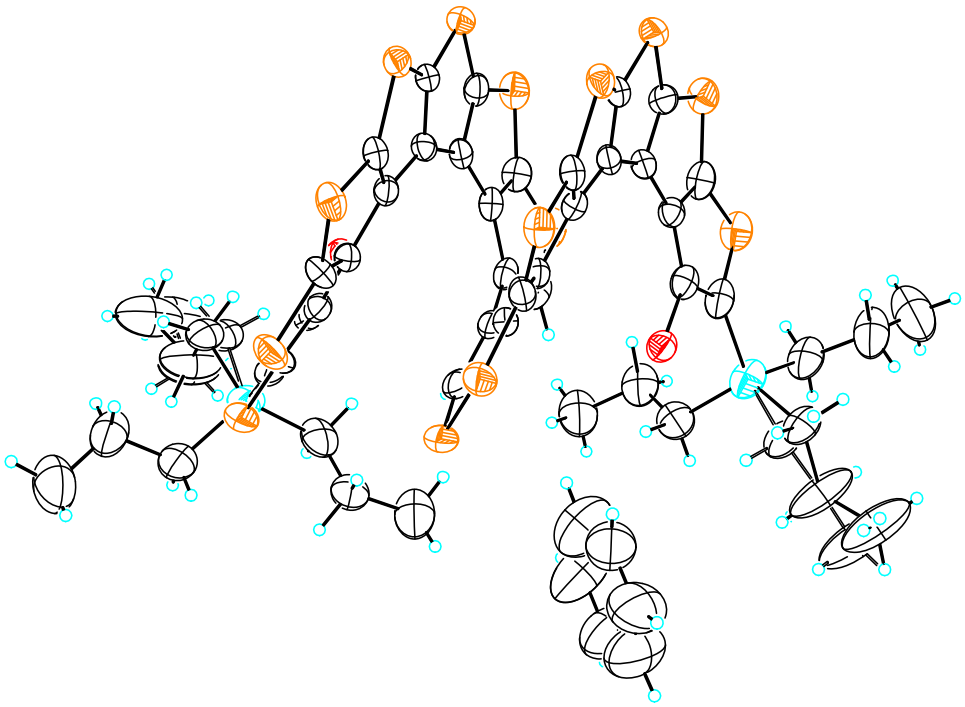

Formula unit, disorder and solvent shown.

Figure S1. Molecular structure and conformation for tetrakis(β-trithiophene) **1** (top) and bis[7]helicene **2** (bottom): formula unit, with all disorder and solvent shown. Carbon, bromine, silicon, and sulfur atoms are depicted with thermal ellipsoids set at the 50% probability level.

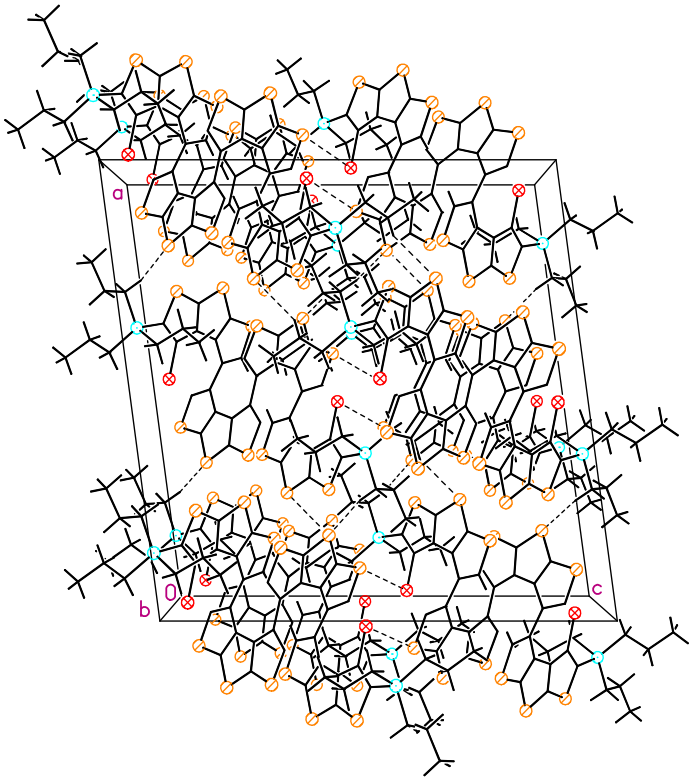

Cell plot, view along *b*.

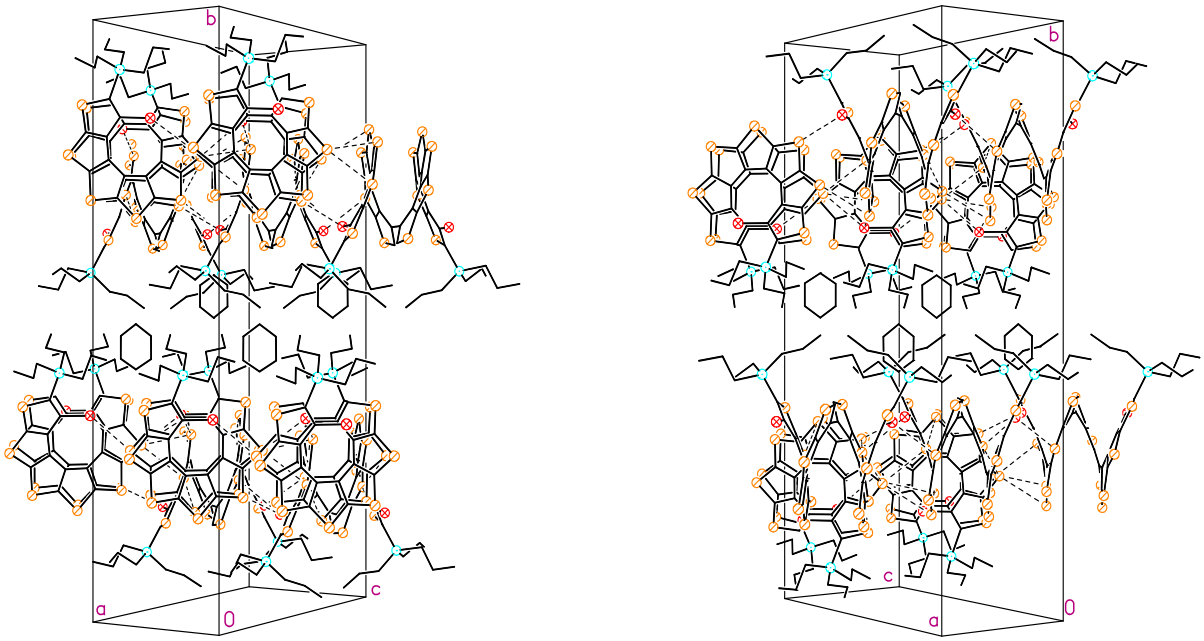

Cell plots, views at (1 0 1) and (1 0 -1)

Figure S2. Selected plots for crystal packing for tetrakis(β-trithiophene) **1** (top, view along *b*) and bis[7]helicene **2** (bottom, views at (1 0 1) and (1 0 -1).

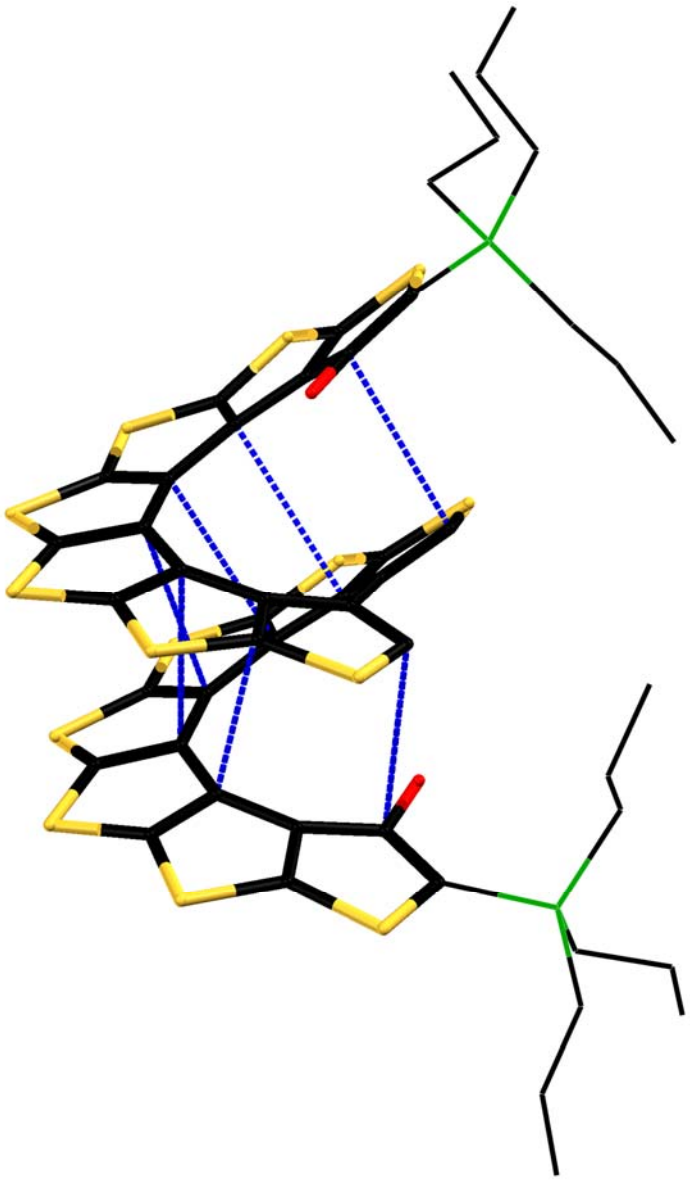

Figure S3. Enlarged version of Figure 2e in the main text, showing helically-locked bis[7]helicene **2** as a molecular hinge: short intramolecular C…C (3.23–3.30 Å) distances between the [7]helicene moieties that are at least 0.1 Å below the sum of the van der Waals radii. Other short distances are summarized in Table S1.

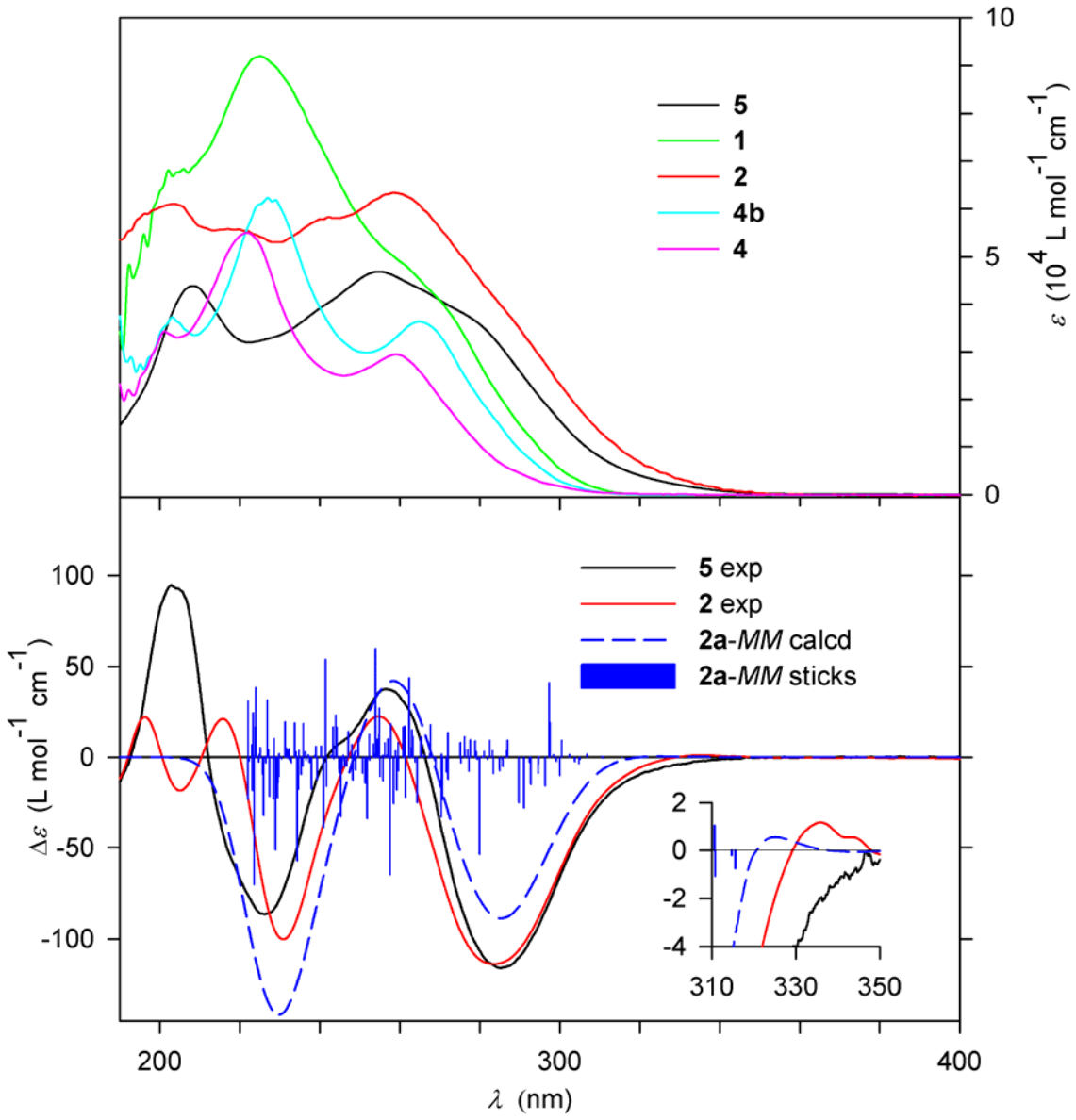

Figure S4. Expanded version of Figure 3 in the main text, with the experimental UV-vis absorption spectra. Electronic CD and UV-vis absorption spectra for bis[7]helicene **2**, its synthetic intermediates, and [7]helicene **5**[S6] in cyclohexane (solid lines). The blue dash lines and sticks correspond to the calculated CD spectrum for bis[7]helicene **2a** at the TD-B3LYP/6-31G(d) level with the IEF-PCM-UAHF solvent model for cyclohexane; the ground state geometry is optimized at the B3LYP/6-31G(d) level in the gas phase. Top plot: UV-vis spectra. Bottom plot including inset: CD spectra.

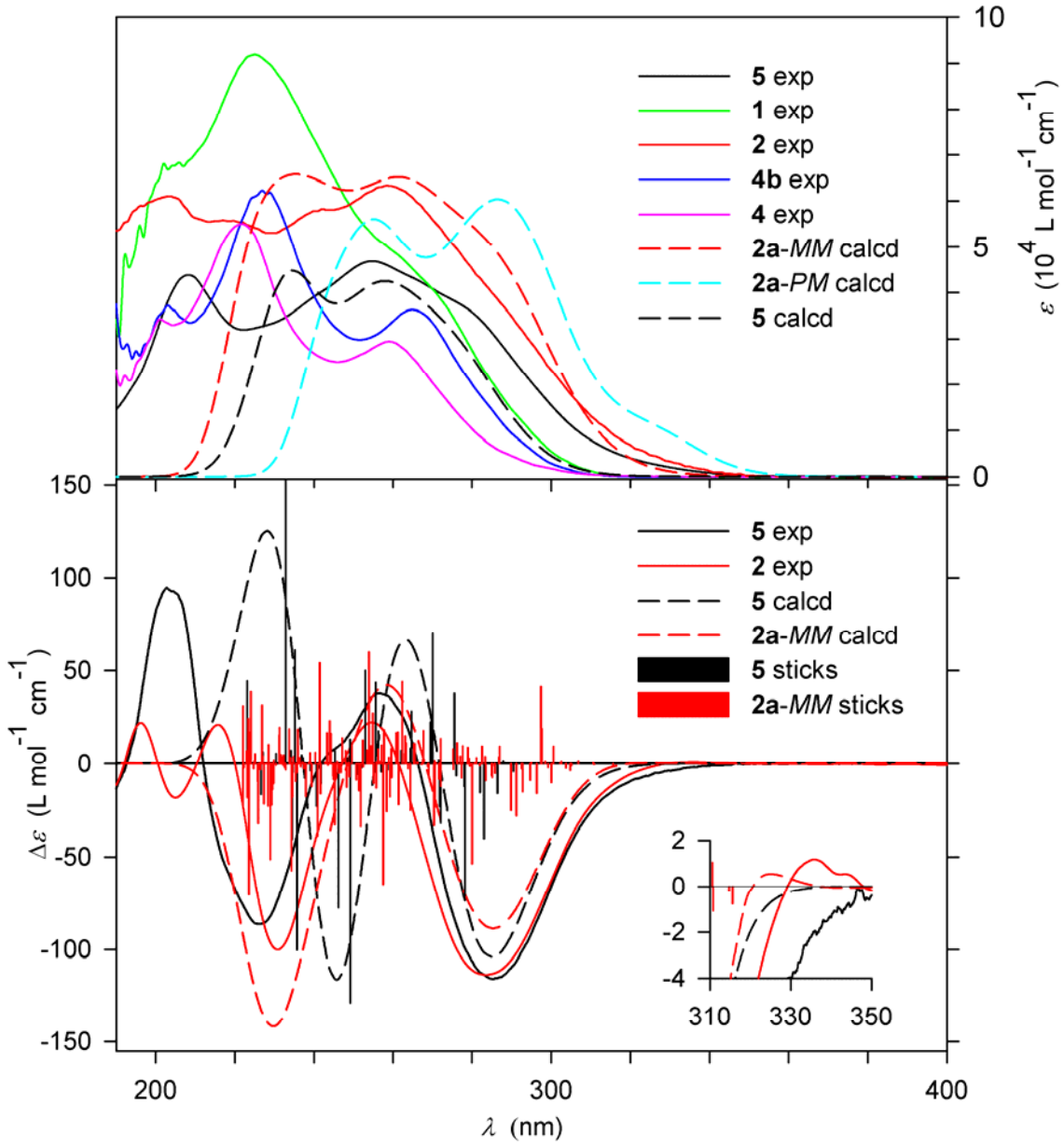

Figure S5. UV-vis (top plots) and CD (bottom plots). Experimental and calculated spectra are shown in solid and dash lines, respectively. The spectra are calculated at the TD-B3LYP/6-31G(d) level using IEF-PCM-UAHF solvent model for cyclohexane; ground state geometries are optimized at the B3LYP/6-31G(d) level (gas phase).

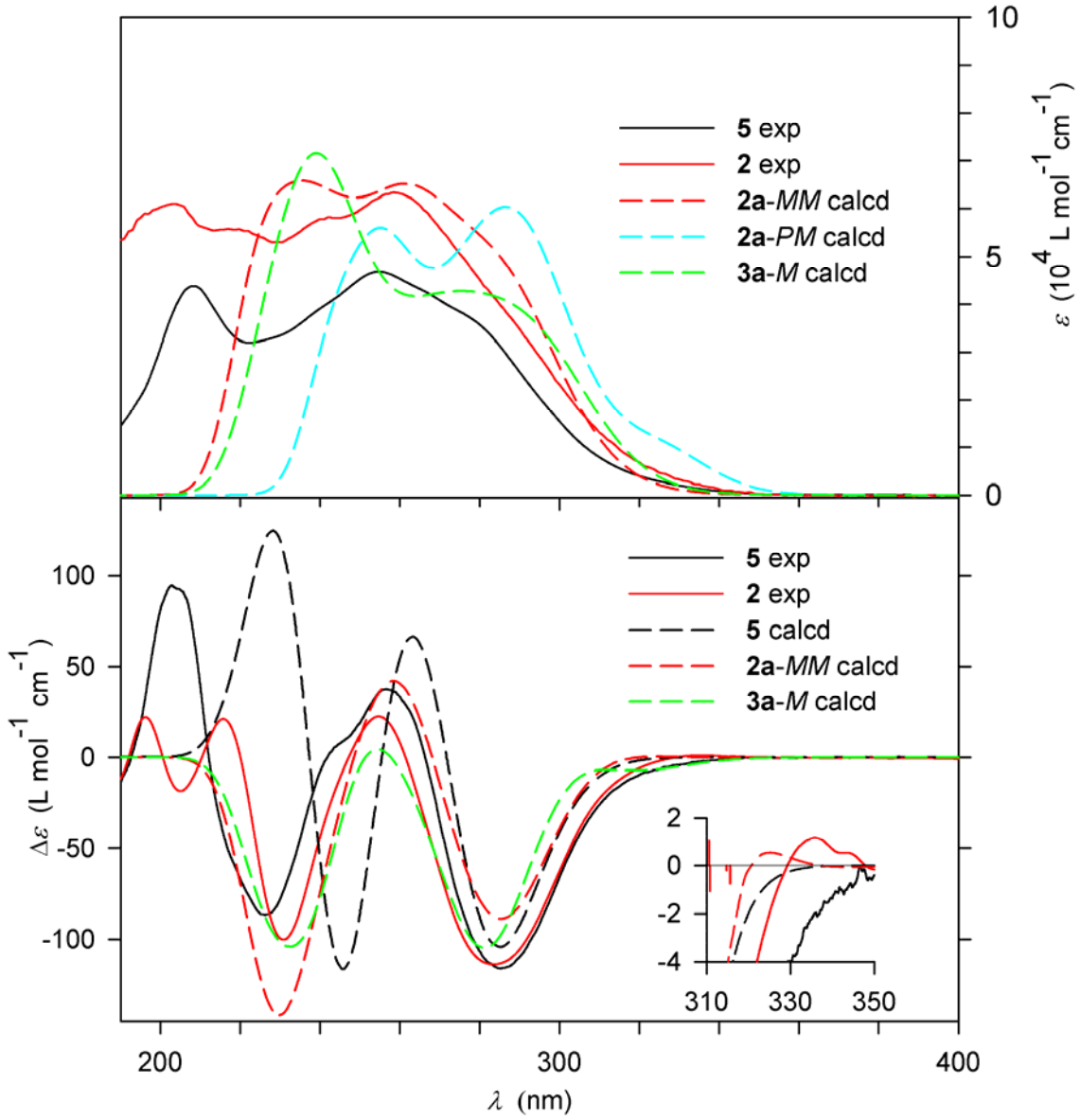

Figure S6. UV-vis (top plots) and CD (bottom plots) electronic spectra: comparison between [7]helicene **5** (plotted as *M*-configuration), bis[7]helicenes **2** and **2a** (*MM*-configuration*)* and **2a**-*PM*, and [15]helicene **3a** (*M*-configuration). Experimental and calculated spectra are shown in solid and dash lines, respectively. The spectra are calculated at the TD-B3LYP/6-31G(d) level using IEF-PCM-UAHF solvent model for cyclohexane; ground state geometries are optimized at the B3LYP/6-31G(d) level (gas phase).

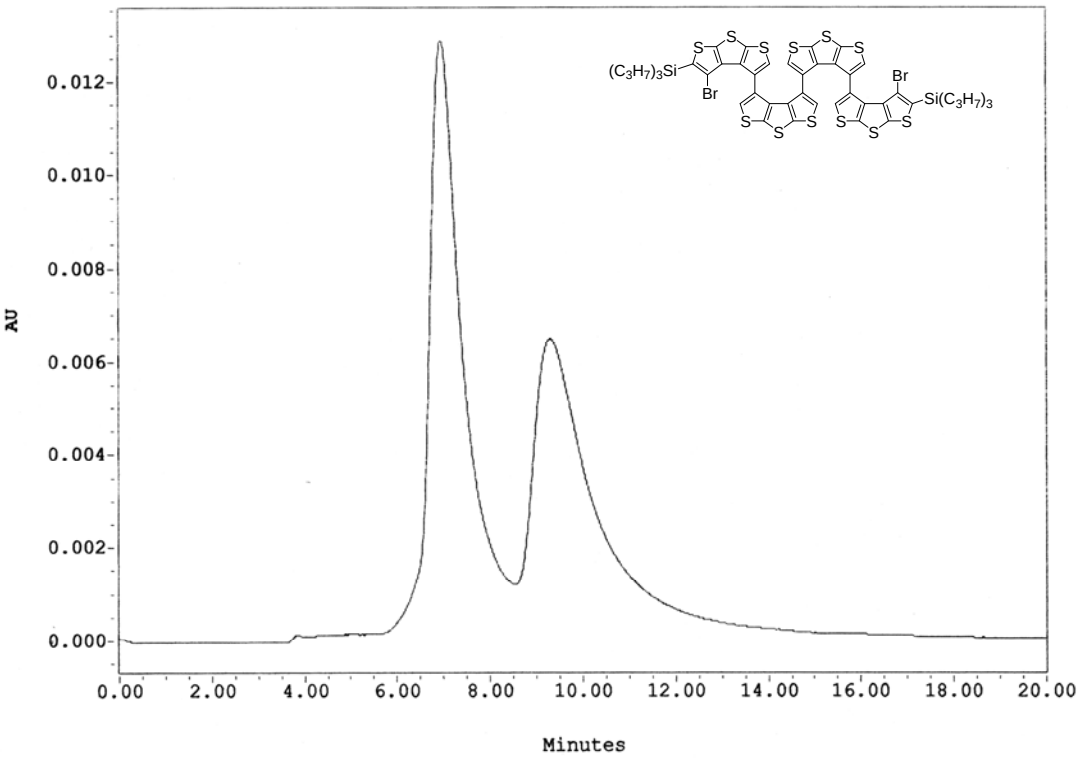

Figure S7. Chiral HPLC of tetrakis(β-trithiophene) **1** (label: MM-19-39-2, eluent: hexane).

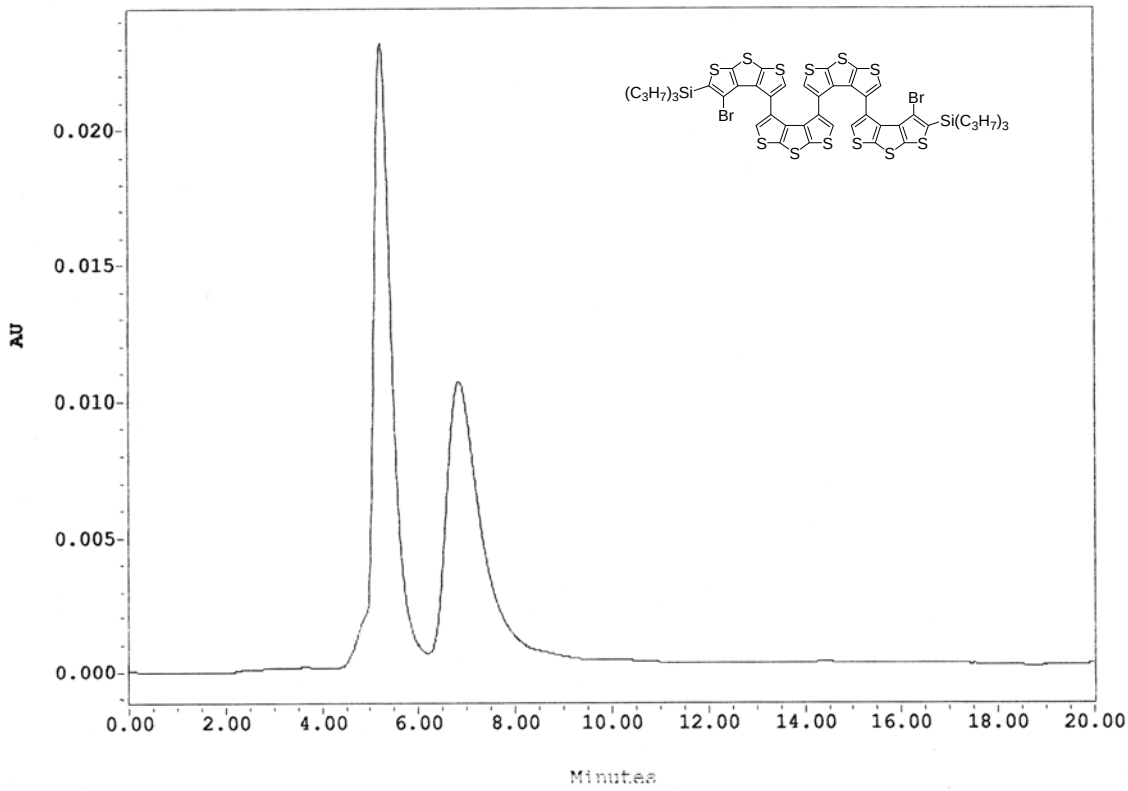

Figure S8. Chiral HPLC of tetrakis(β-trithiophene) **1** (label: MM-19-71-solid, eluent: hexane/*i*-PrOH, 99.5:0.5).

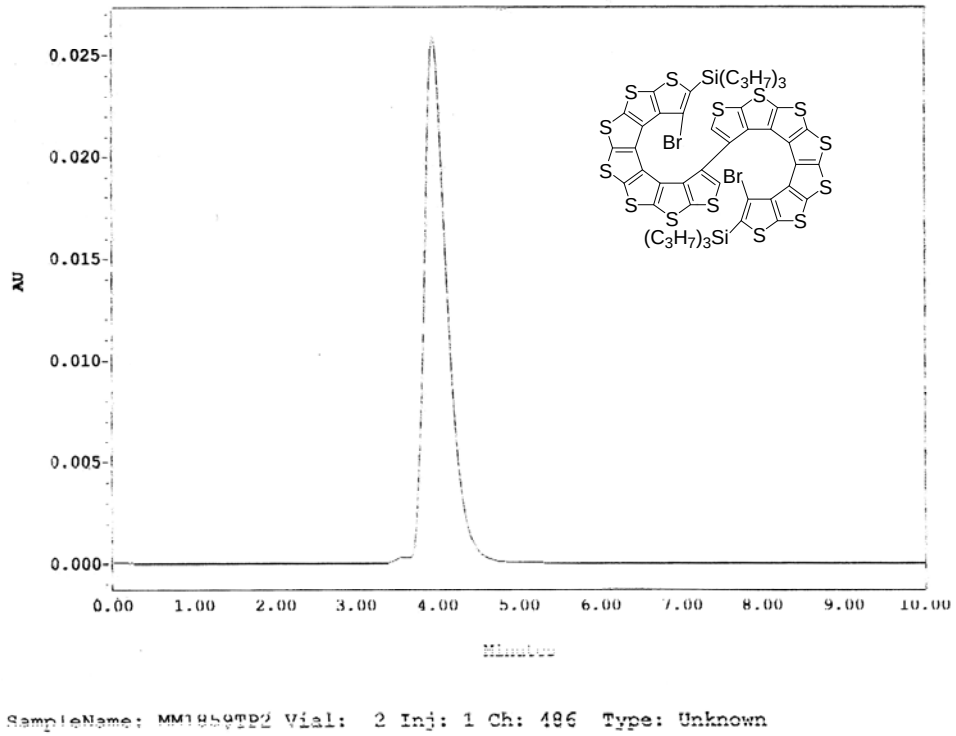

Figure S9. HPLC of bis[7]helicene **2** (label: MM-18-59-TP2, eluent: hexane/*i*-PrOH, 99:1).

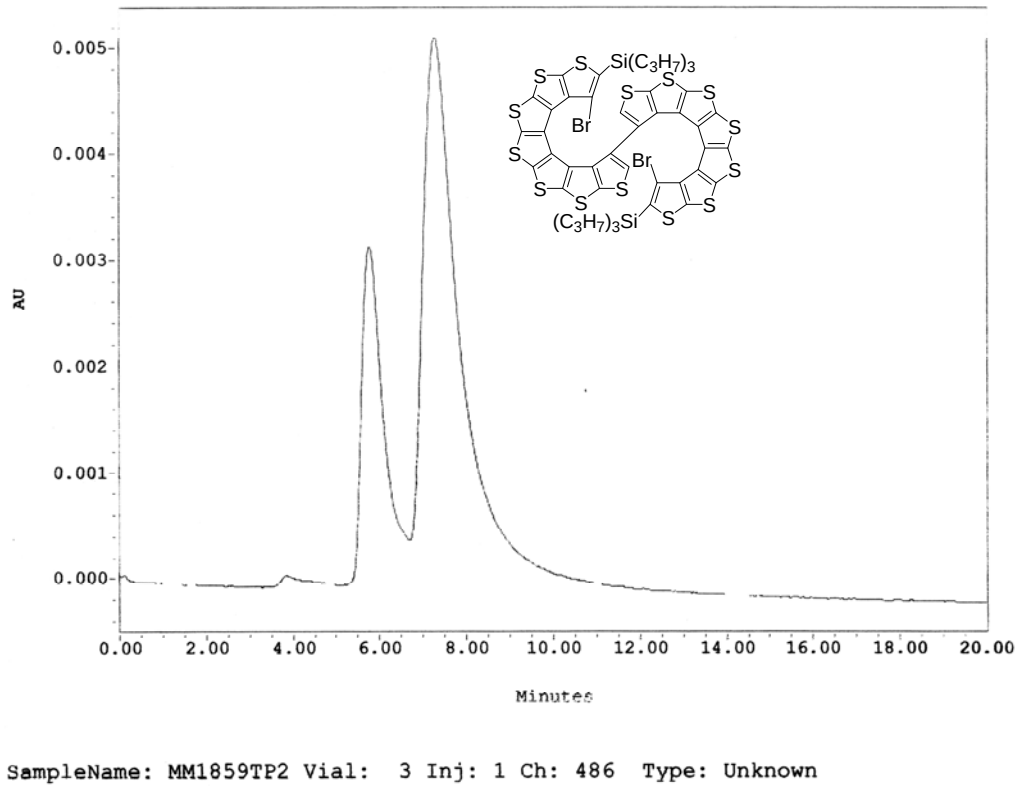

Figure S10. HPLC of bis[7]helicene **2** (label: MM-18-59-TP2, eluent: hexane).

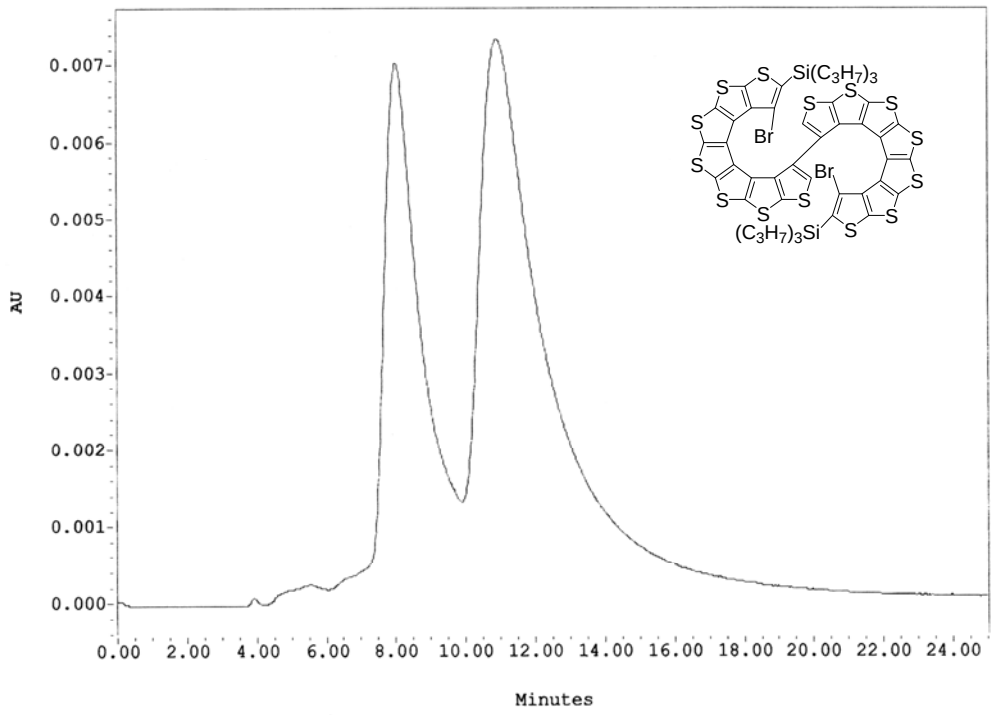

SampleName: MM19602 Vial: 3 Inj: 1 Ch: 486 Type: Unknown

Figure S11. HPLC of bis[7]helicene **2** (label: MM-19-60-2, eluent: hexane).

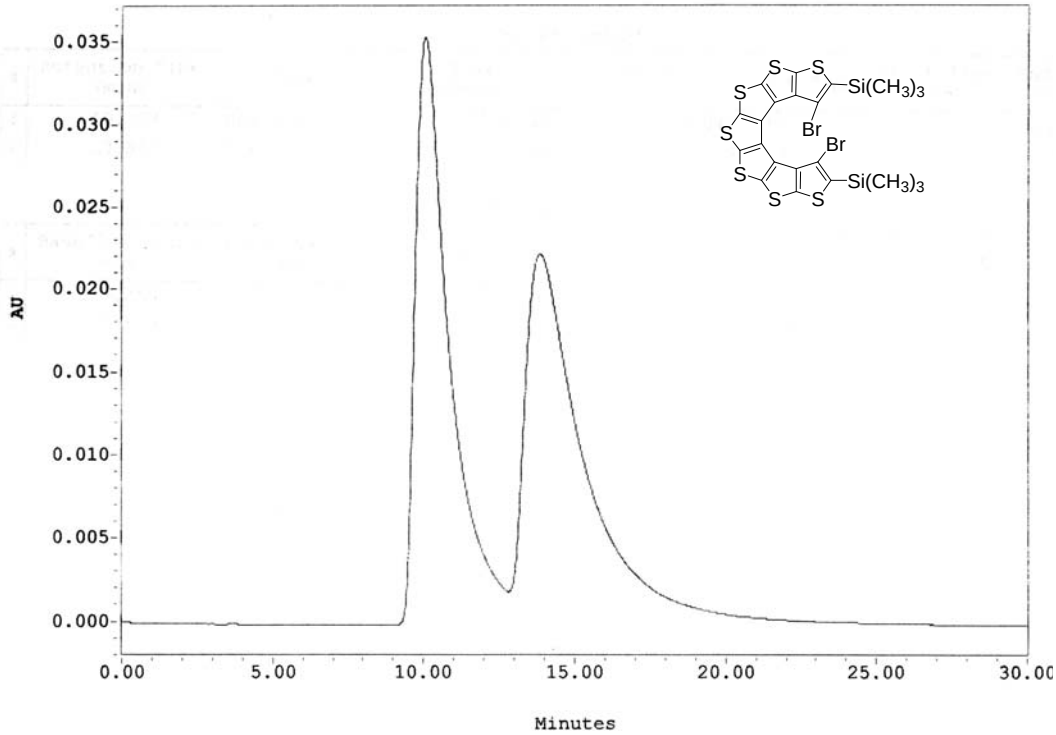

SampleName: MM-21-40-1 Vial: 3 Inj: 1 Ch: 486 Type: Unknown

Figure S12. HPLC of reference [7]helicene **5** (label: MM-21-40-1, eluent: hexane).

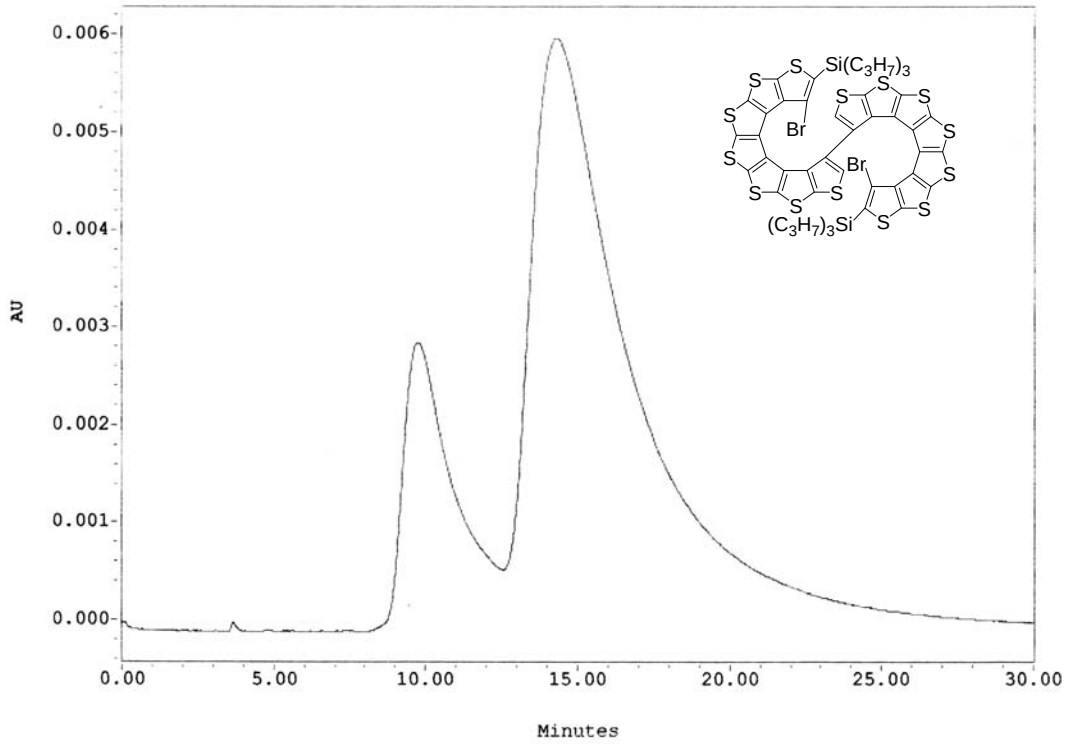

Figure S13. HPLC of bis[7]helicene **2** (label: MM-21-15-TP3-A+B-1+2-TP1-solid, eluent: hexane).

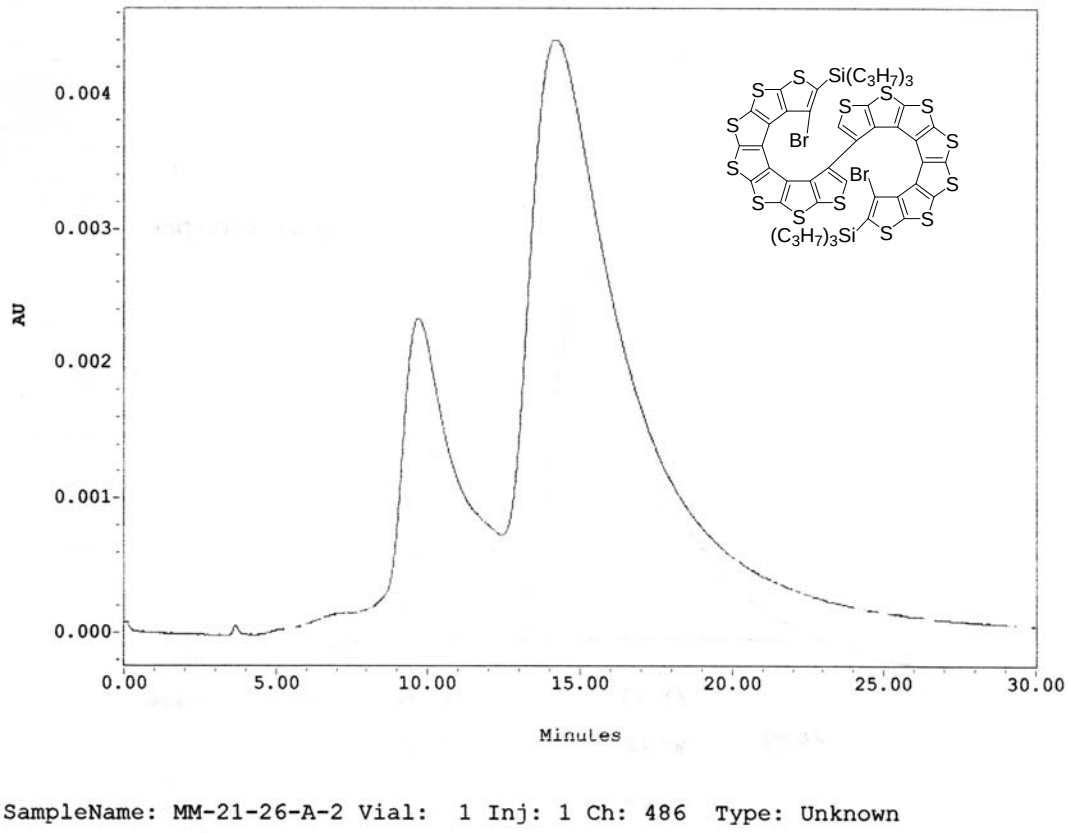

Figure S14. HPLC of bis[7]helicene **2** (label: MM-21-26-TP2+TP3-A-2, eluent: hexane).

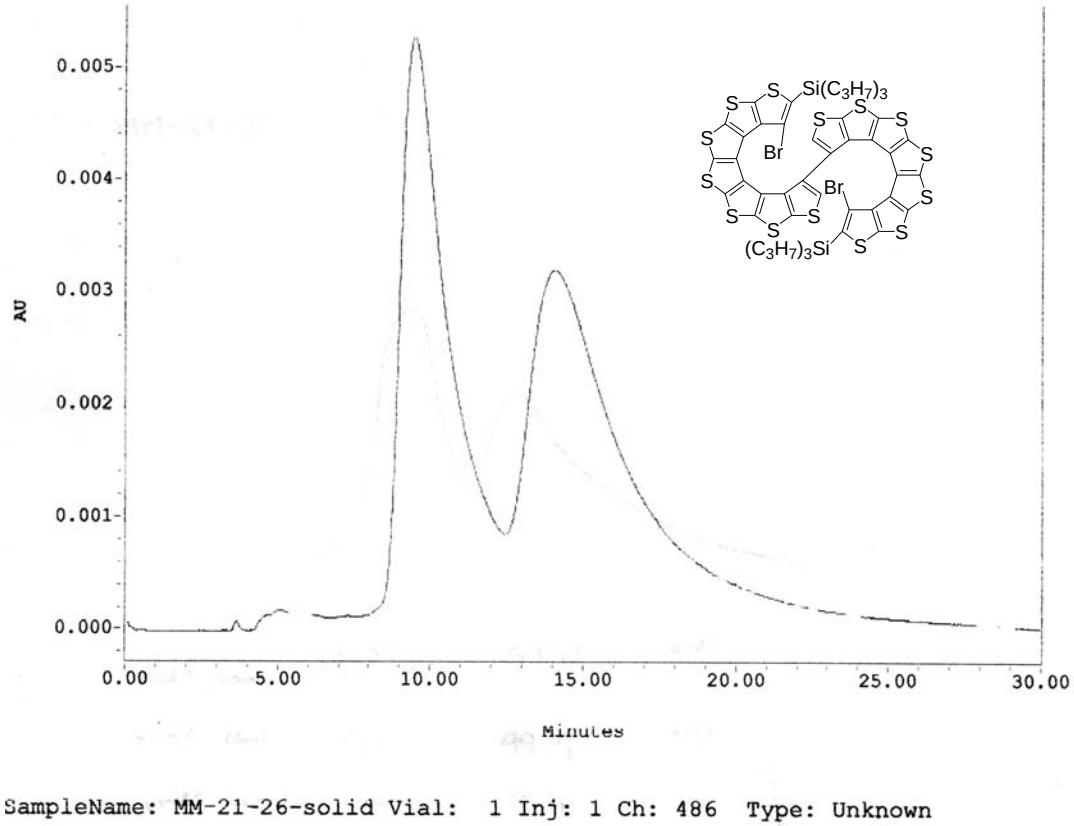

Figure S15. HPLC of bis[7]helicene **2** (label: MM-21-26-TP2+TP3-A-4+5-solid, eluent: hexane).

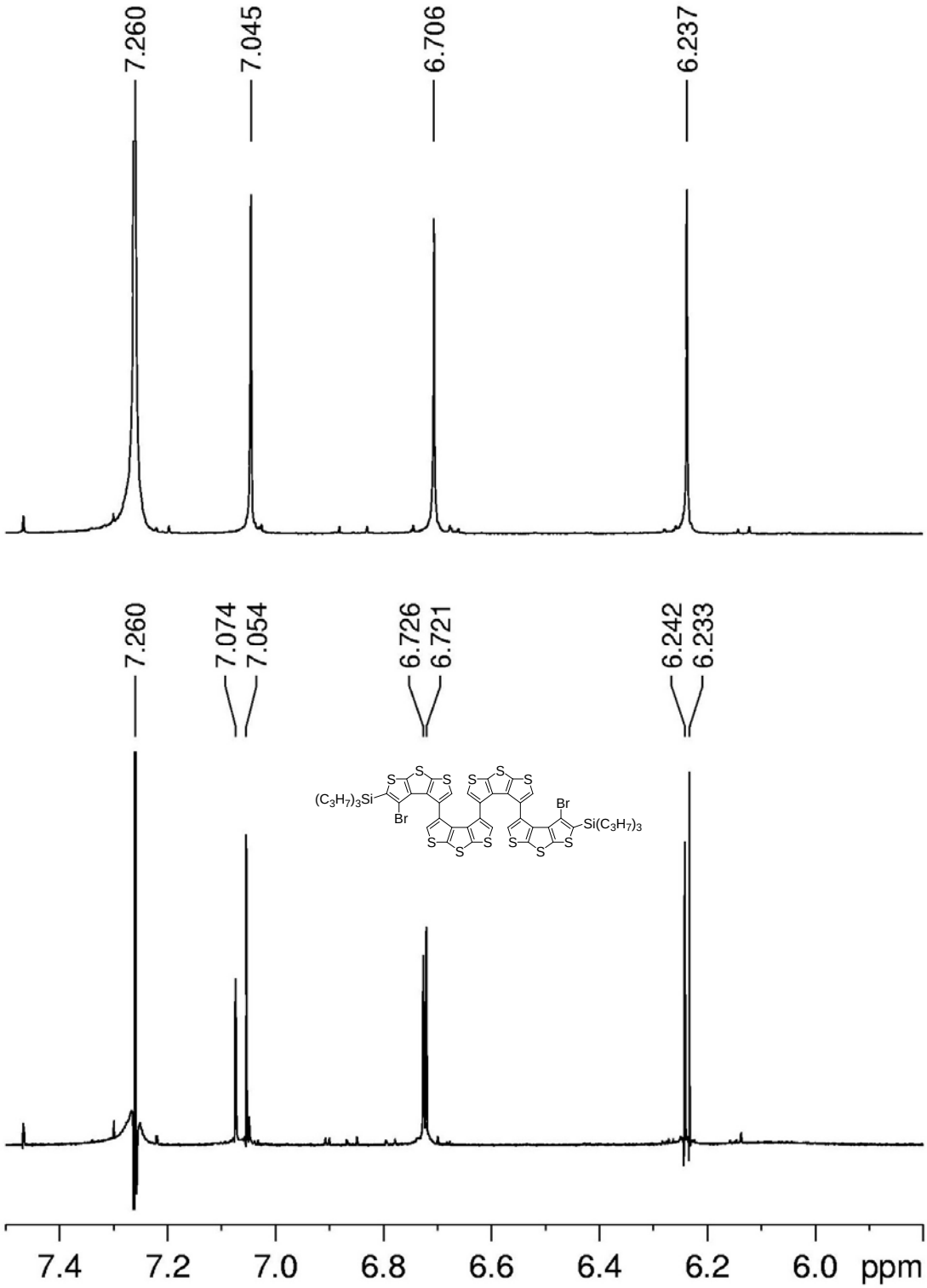

Figure S16. ^{1}H NMR (500 MHz, chloroform-*d*) spectra of tetrakis(β-trithiophene) **1** (0.8 mg) with chiral shift reagents (Yb(hfpc)/Ag(fod)). Top spectrum: before addition of shift reagents (MM-19-25+28-col-2-solid-1). Bottom spectrum: after addition of shift reagents, Yb(hfpc) = 2.2 mg, Ag(fod) = 2.7 mg, and resolution enhancement, LB = −0.8, GB = 0.4 (MM-19-25+28-col-2-solid-4).

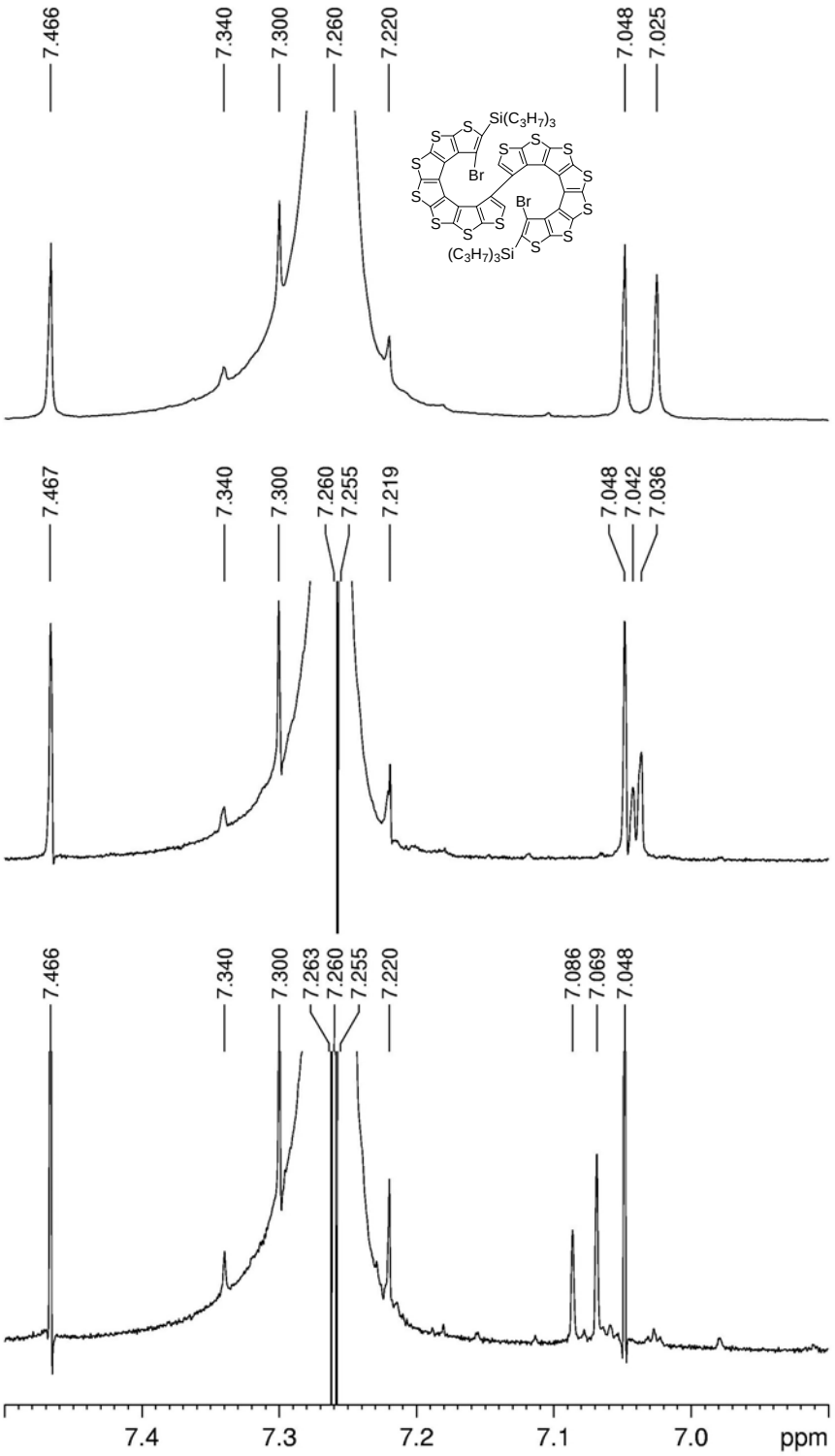

Figure S17. ^{1}H NMR (500 MHz, chloroform-*d*) spectra of bis[7]helicene **2** (~0.3 mg) with chiral shift reagents (Yb(hfpc)/Ag(fod)). Top spectrum: before addn of shift reagents (MM-19-57-TP2-$CDCl_3$). Middle spectrum: after first addn of shift reagents, Yb(hfpc) = 1.1 mg, Ag(fod) = 1.3 mg, LB = −0.5, GB = 0.3 (MM-19-57-TP2-1). Bottom spectrum: after subsequent addn(s) of shift reagents, Yb(hfpc) = 3.7 mg, Ag(fod) = 4.1 mg, LB = −0.6, GB = 0.3 (MM-19-57-TP2-3).

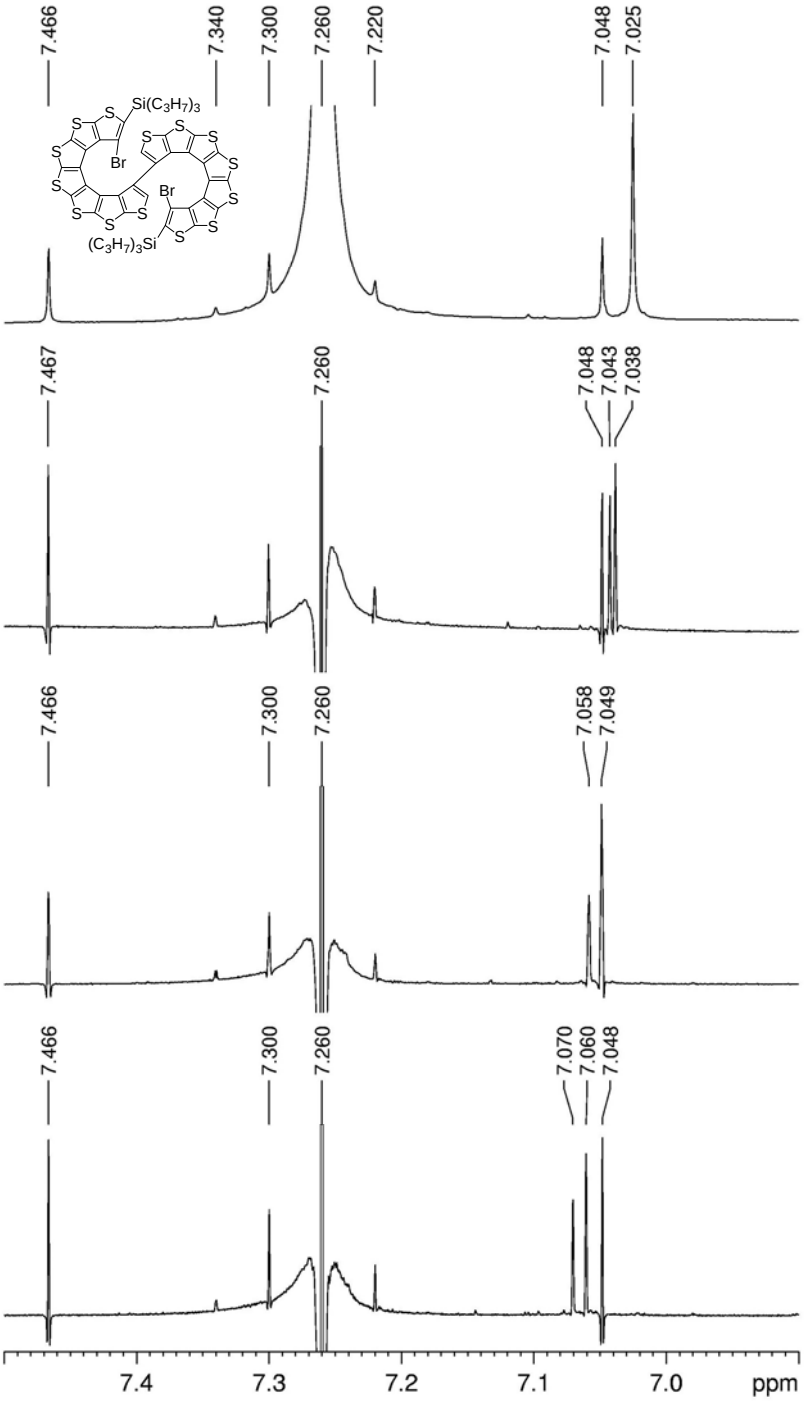

Figure S18. ^{1}H NMR (500 MHz, chloroform-*d*) spectra of bis[7]helicene **2** (0.4 mg) with chiral shift reagents (Yb(hfpc)/Ag(fod)). Top-to-bottom spectra: before addn of shift reagents and then after addns of increased amounts of shift reagents. Top: MM-19-59-1. Second from top: MM-19-59-2, Yb(hfpc) = 0.7 mg, Ag(fod) = 1.2 mg, LB = −0.8, GB = 0.4. Third from top: MM-19-59-3, Yb(hfpc) = 1.9 mg, Ag(fod) = 2.0 mg, LB = −0.8, GB = 0.4. Bottom: MM-19-59-4, Yb(hfpc) = 2.8 mg, Ag(fod) = 3.0 mg, LB = −0.8, GB = 0.4.

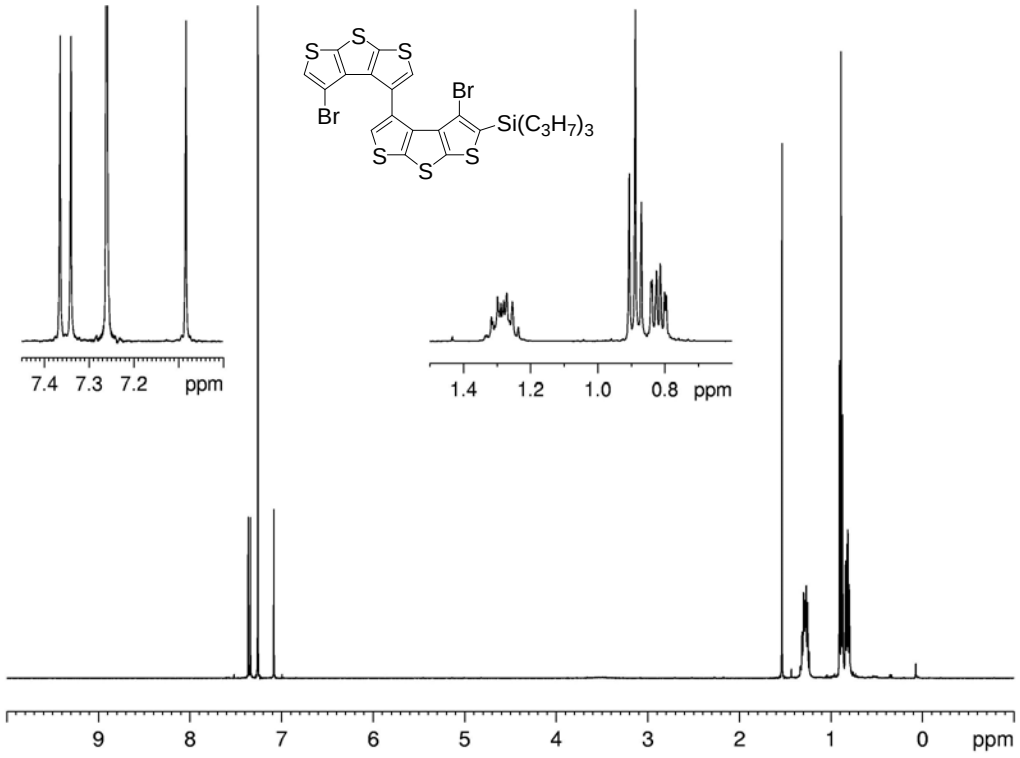

Figure S19. ^{1}H NMR (400 MHz, chloroform-*d*) spectrum of **4a**.

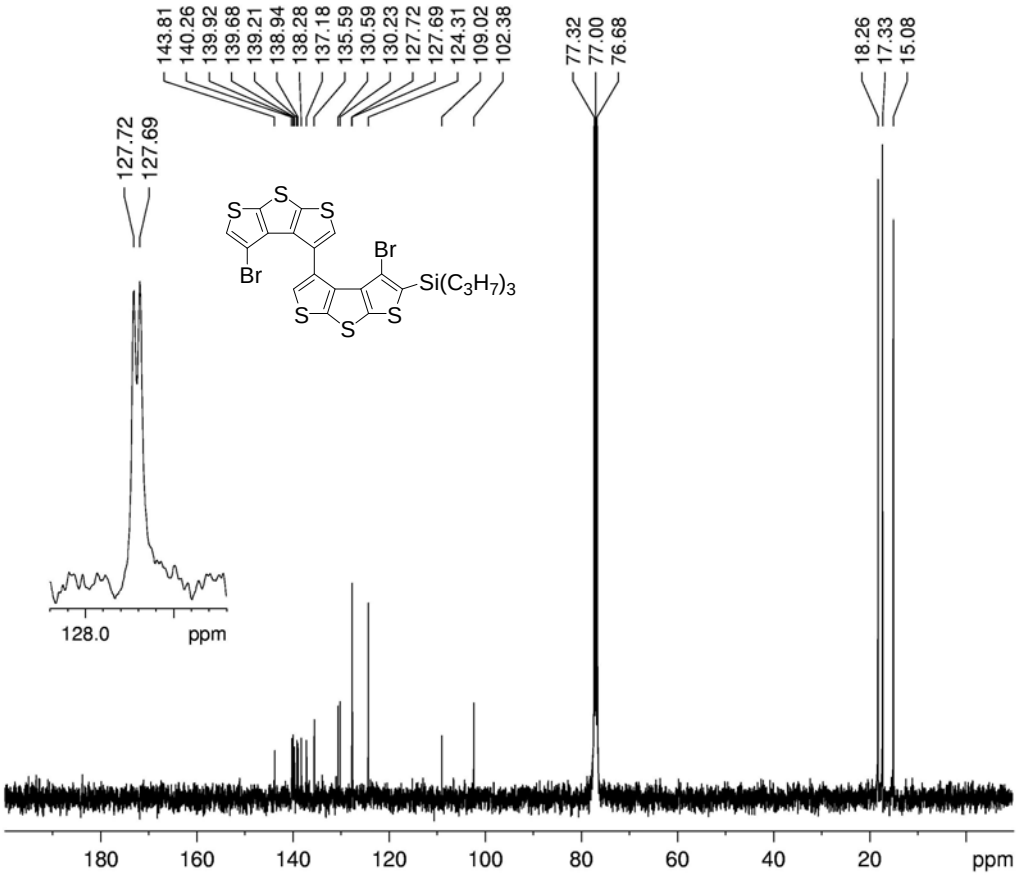

Figure S20. ^{13}C NMR (100 MHz, chloroform-*d*) spectrum of **4a**.

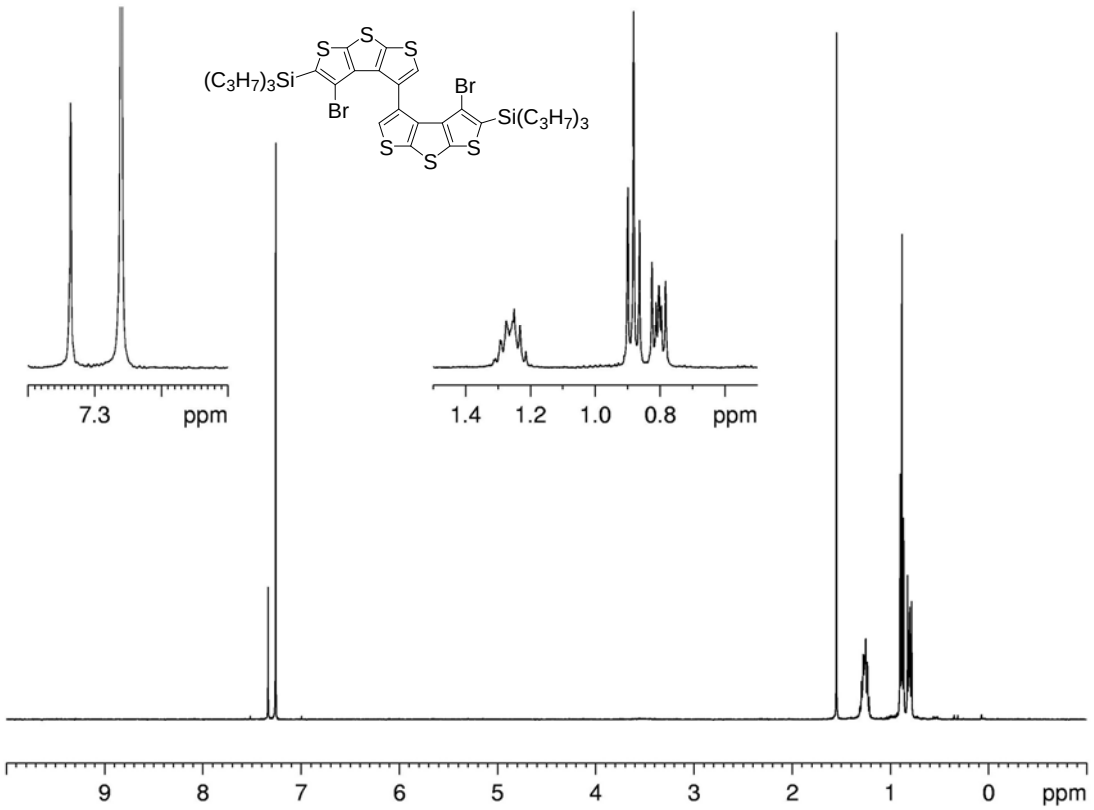

Figure S21. ^{1}H NMR (400 MHz, chloroform-*d*) spectrum of **4b**.

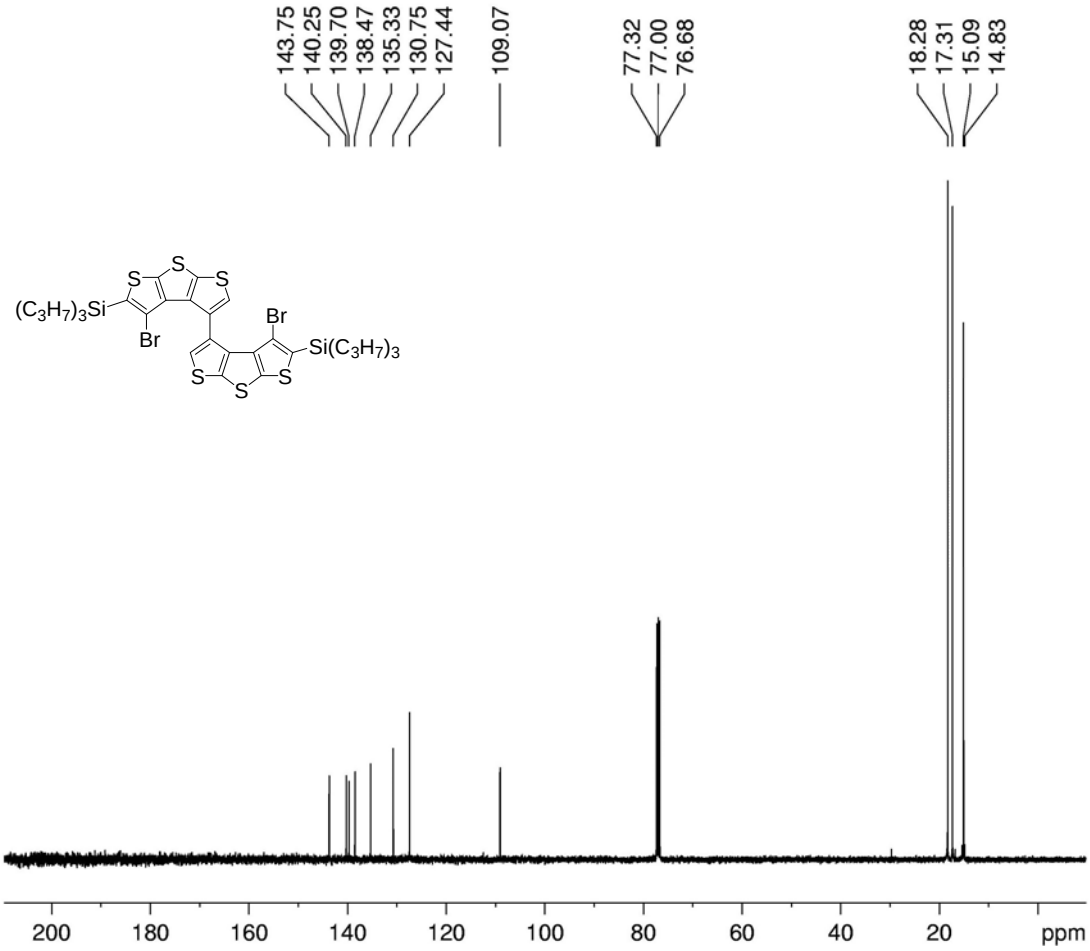

Figure S22. ^{13}C NMR (100 MHz, chloroform-*d*) spectrum of **4b**.

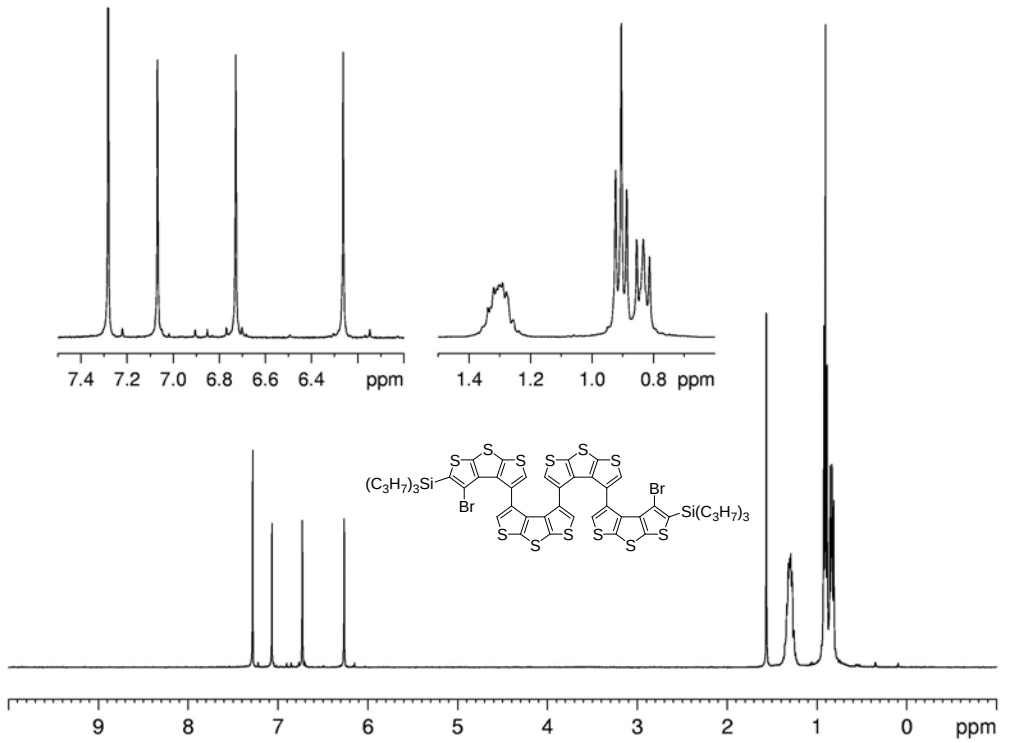

Figure S23. ^{1}H NMR (400 MHz, chloroform-*d*) spectrum of tetrakis(β-trithiophene) **1**.

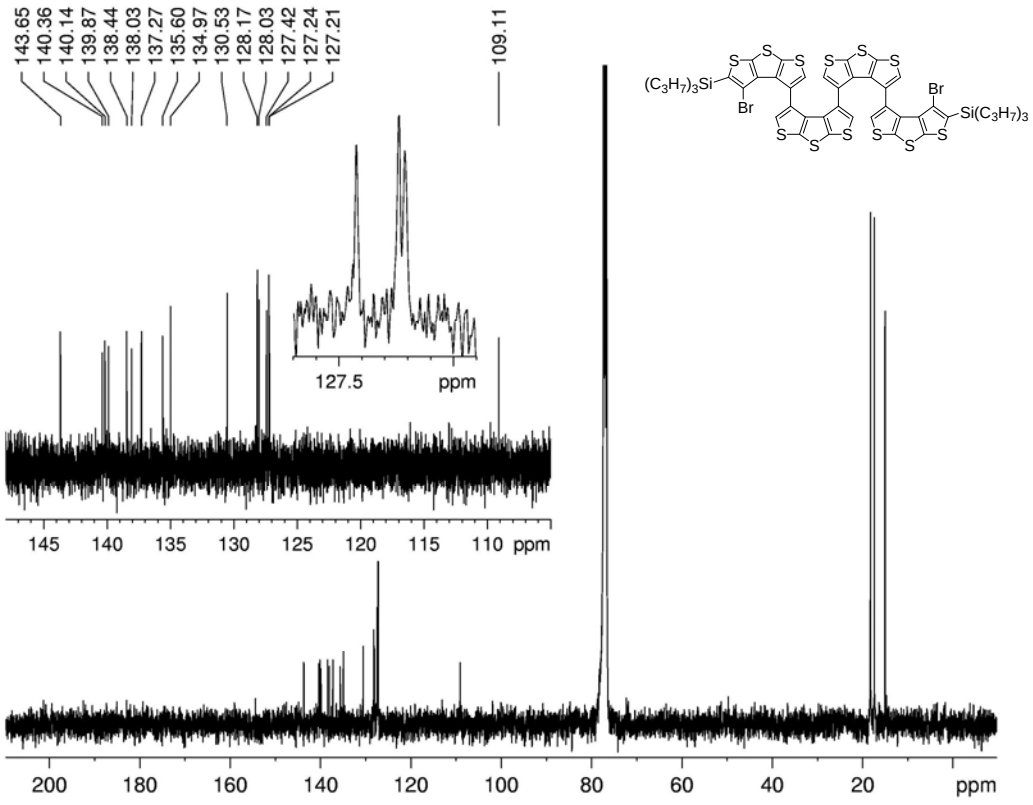

Figure S24. ^{13}C NMR (100 MHz, chloroform-*d*) spectrum of tetrakis(β-trithiophene) **1**.

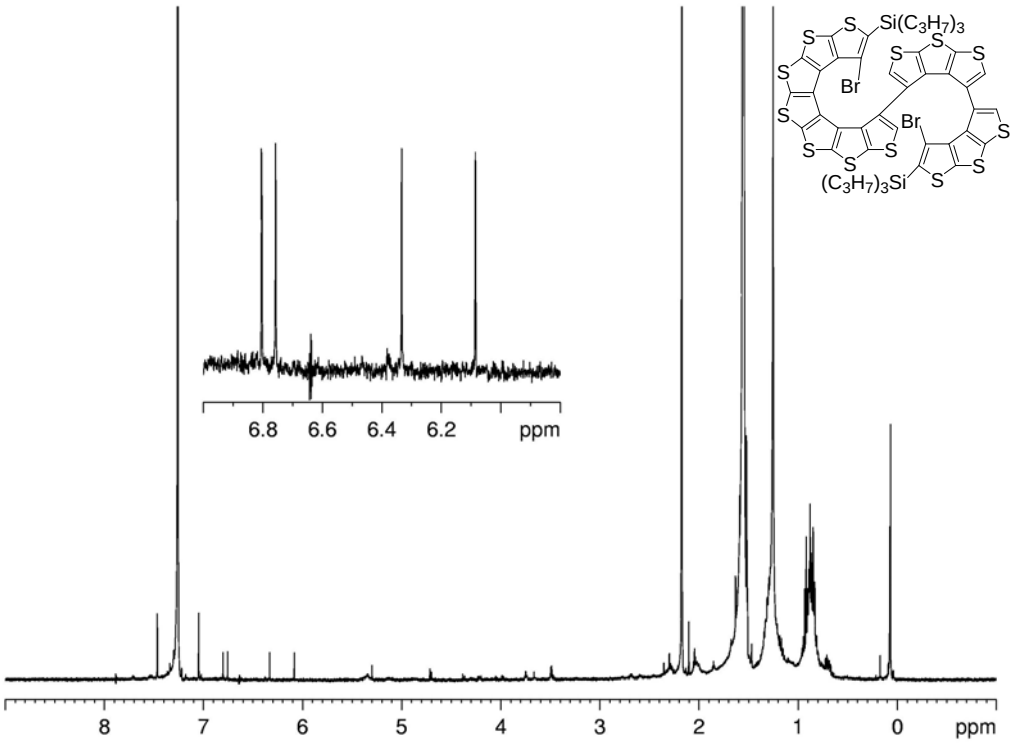

Figure S25. ^{1}H NMR (500 MHz, chloroform-*d*) spectrum of tridecathiophene by-product (MM-15-88-TP3-B).

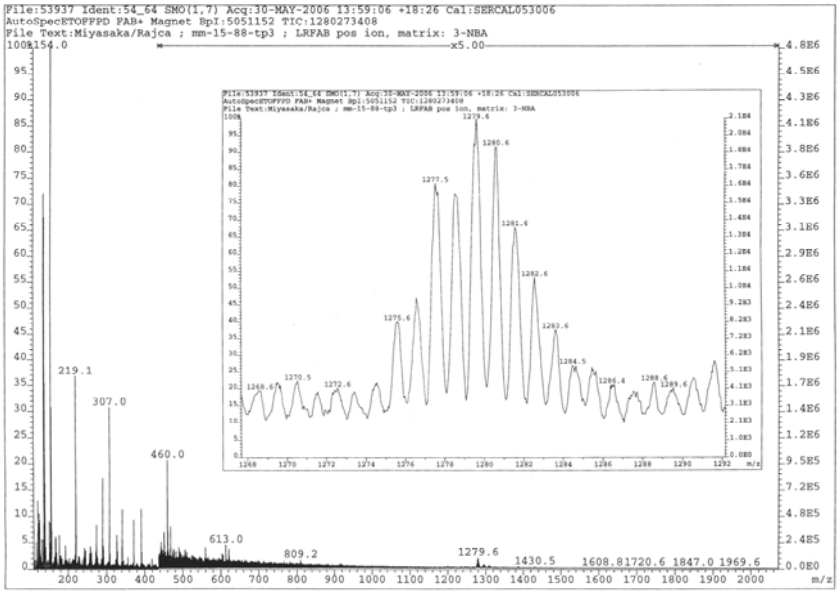

Figure S26. LR FABMS spectrum of tridecathiophene by-product (MM-15-88-TP3-B). The spectrum was vertically expanded by factor of 5 in the *m/z* 440 – 2100 range. Inset spectrum shows the expansion in the *m/z* 1268 – 1292 range.

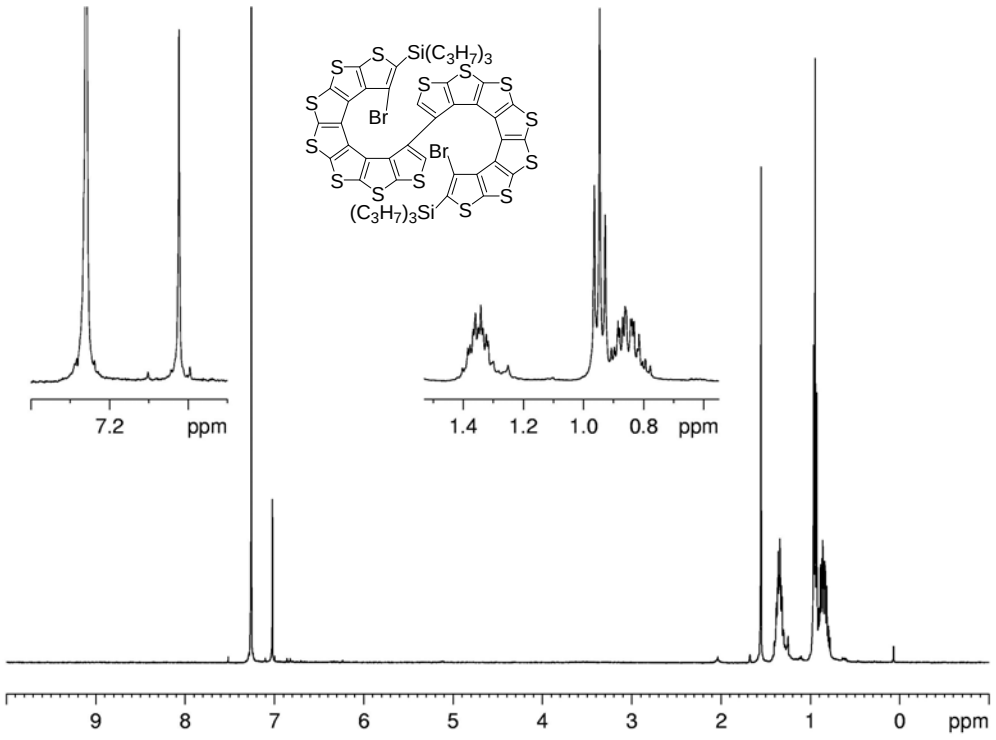

Figure S27. ^{1}H NMR (400 MHz, chloroform-*d*) spectrum of bis[7]helicene **2** (MM-21-26-TP2+TP3-A-4+5-solid).

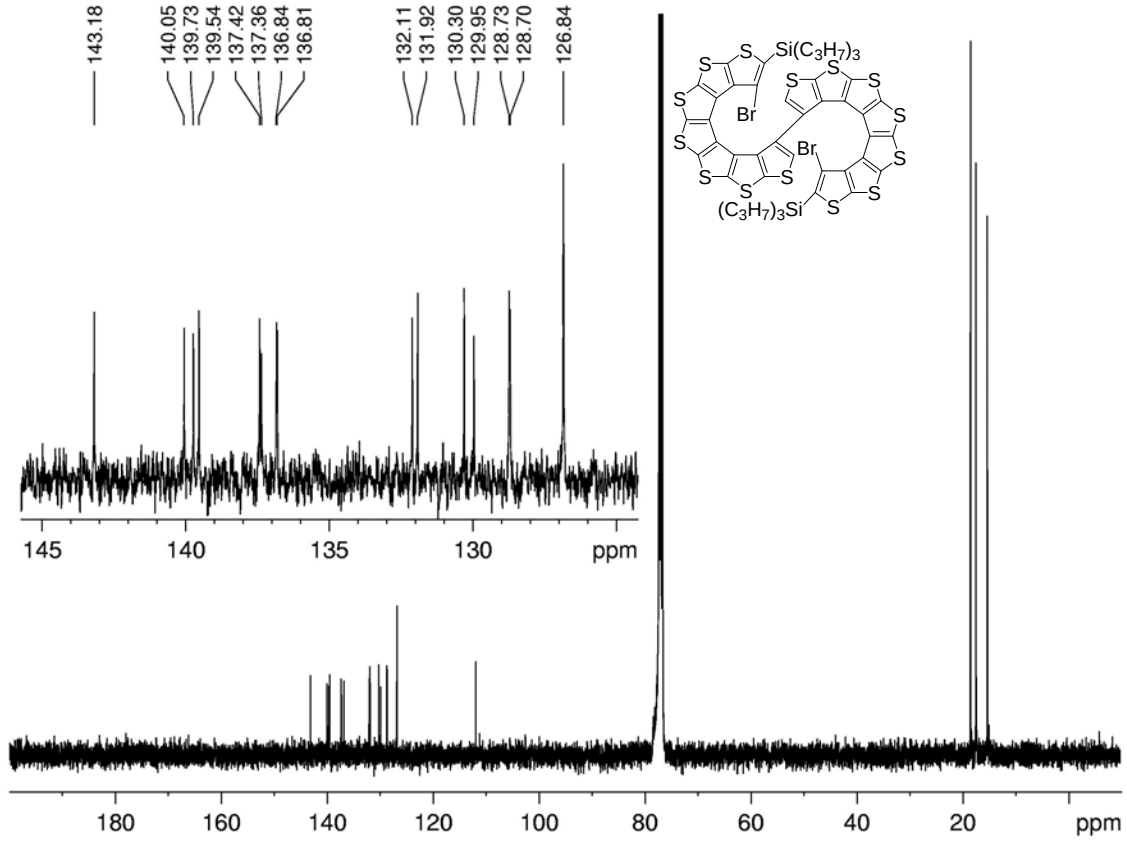

Figure S28. ^{13}C NMR (100 MHz, chloroform-*d*) spectrum of bis[7]helicene **2** (MM-21-26-TP2+TP3-A-4+5-solid).

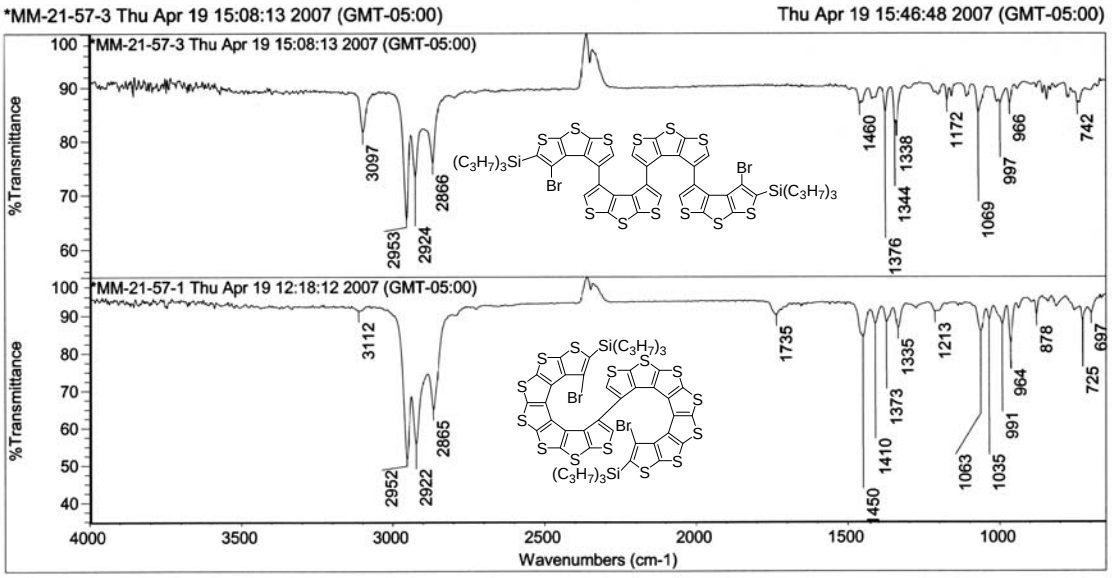

Figure S29. Comparison of IR spectra of tetrakis(β-trithiophene) **1** and bis[7]helicene **2**. These IR spectra were obtained consecutively, starting with bis[7]helicene **2**; 256 scans were acquired for each spectrum.

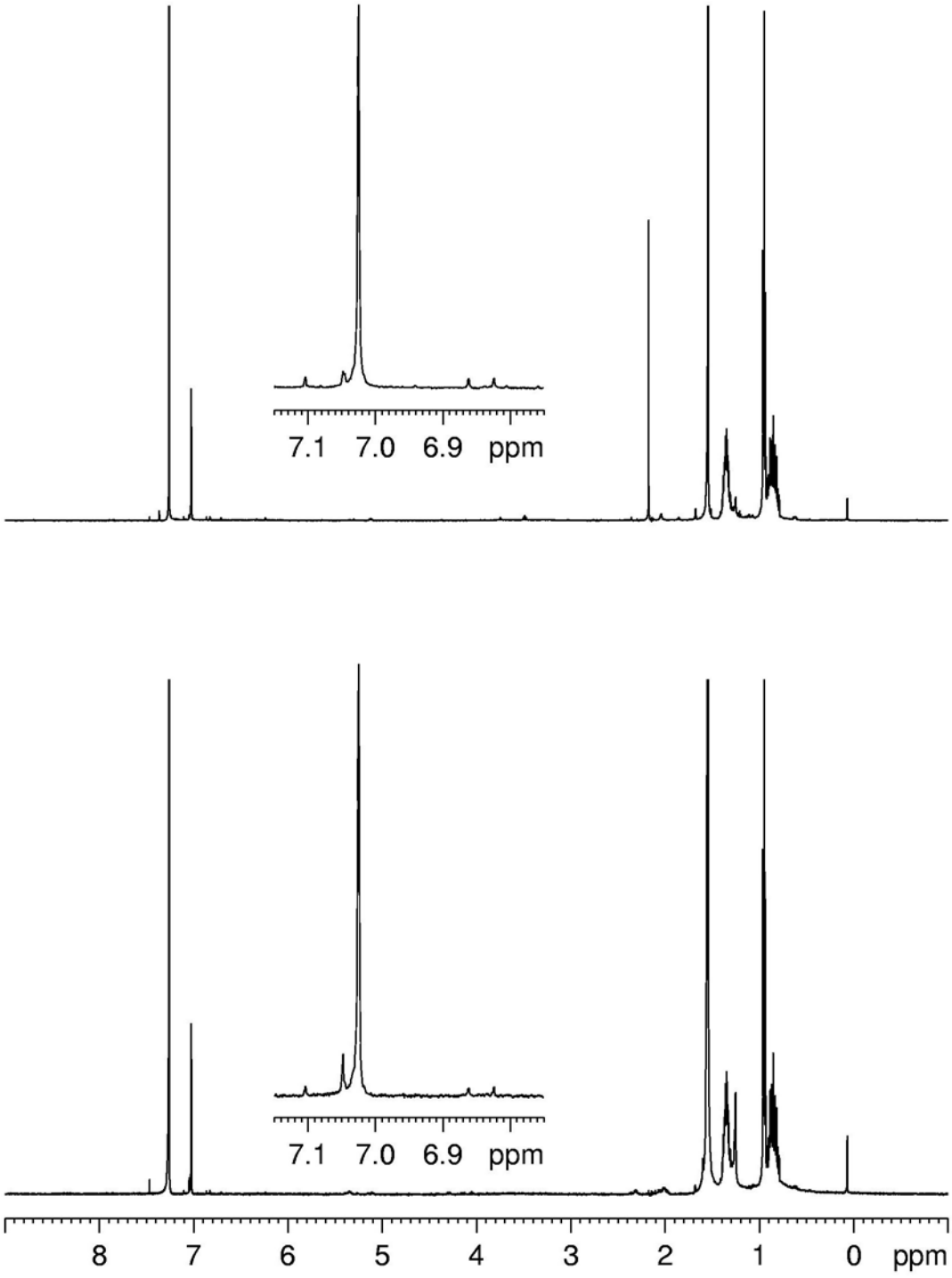

Figure S30. ^{1}H NMR (500 MHz, chloroform-*d*) spectra of **2** (MM-21-26-TP2+TP3-A-4+5-solid). Top spectrum: before heating. Bottom spectrum: after 1 h at 280 °C.

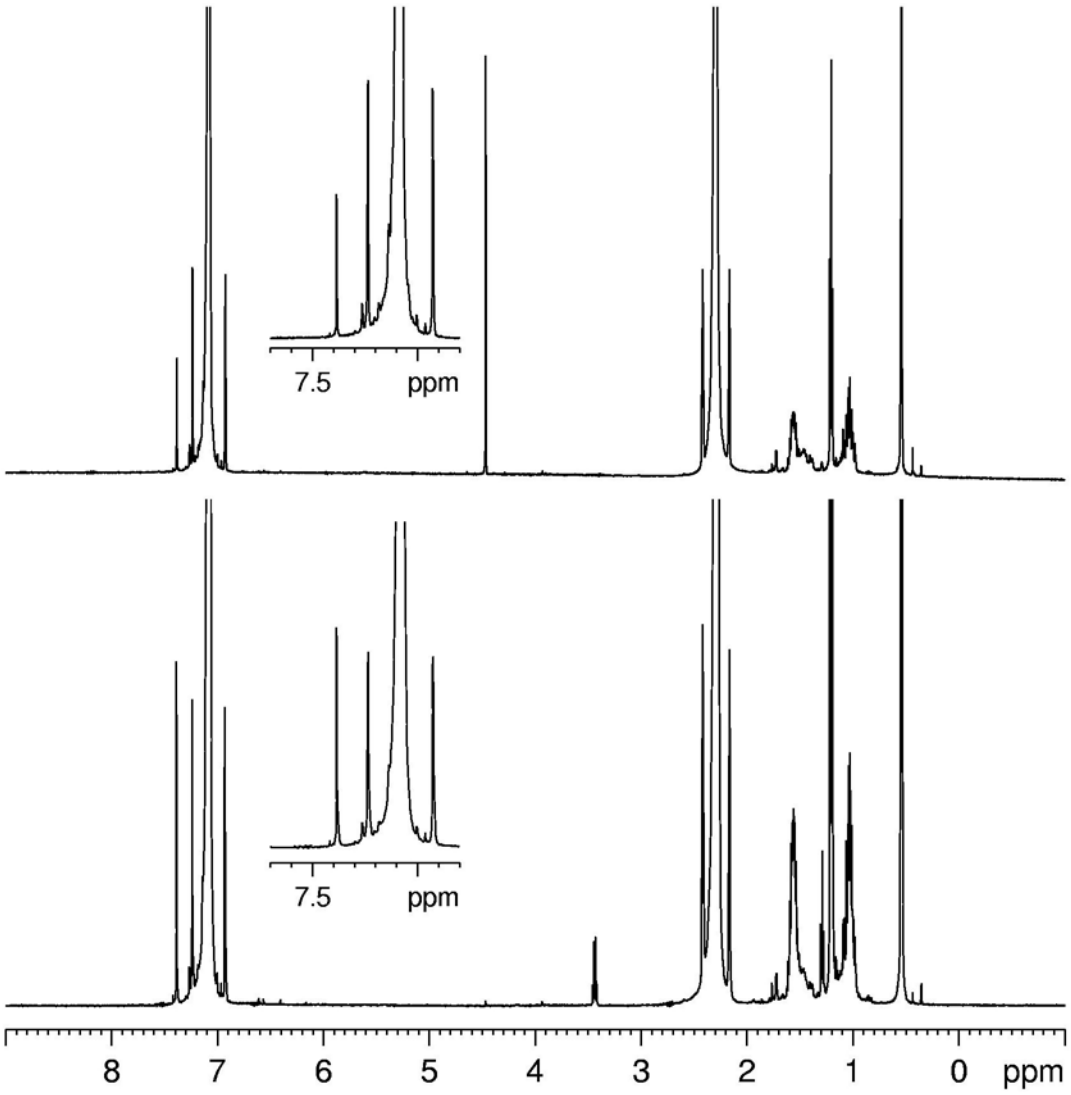

Figure S31. ^{1}H NMR (500 MHz, *p*-xylene-d_{10}) spectra of **2** (MM-21-26-TP2+TP3-A-4+5-solid). Top spectrum: before heating (label: MM-21-56-1H-xylene); the singlet at about 4.8 ppm is most likely due to the residual dichloromethane. Bottom spectrum: after 10 h at 200 °C (label: MM-21-56-2).

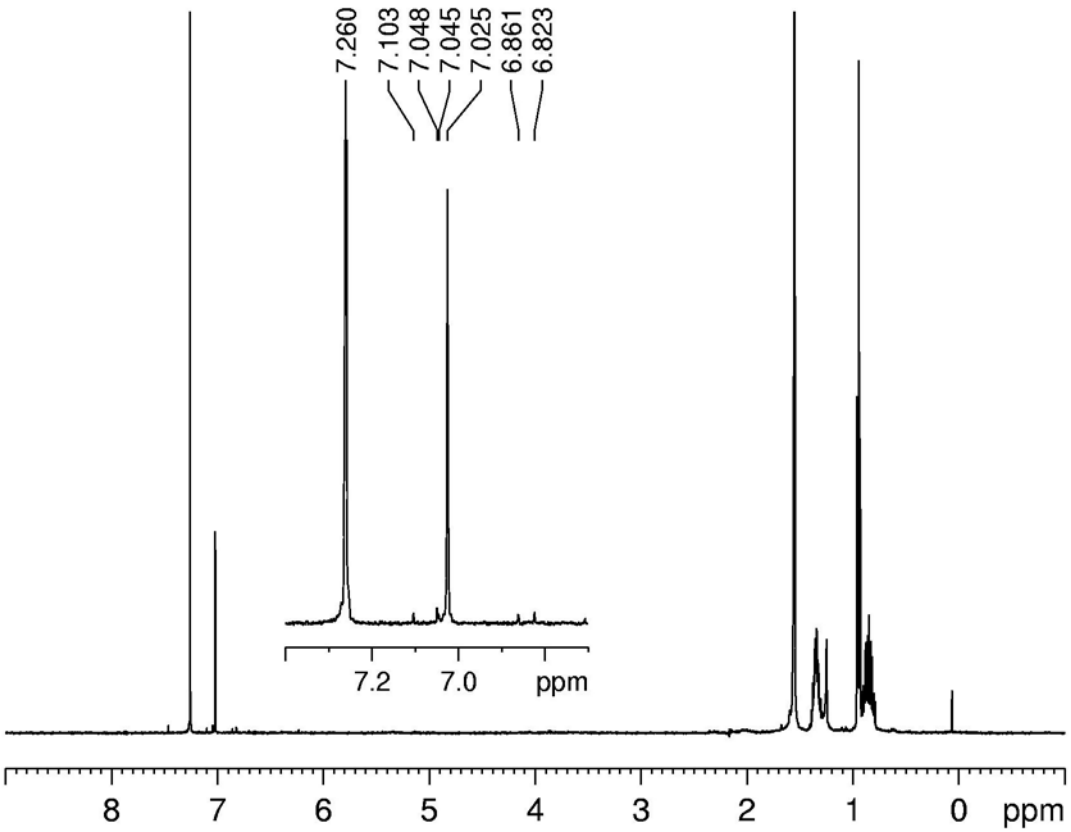

Figure S32. ^{1}H NMR (500 MHz, chloroform-*d*) spectrum of bis[7]helicene **2** after 10 h in *p*-xylene-d_{10} at 200 °C (MM-21-56-2), and then removal of solvent in vacuo (label: MM-21-56-3).

4. Supporting Tables.

Table S1. Selected intramolecular distances (Å) and angles (°) from X-ray structures of tetrakis(β-trithiophene) **1** and bis[7]helicene **2**.

Compound	Distances between β-trithiophene moieties[a]			Torsion angles for β,β-linkages	
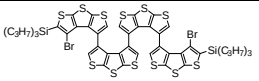 *RRR*	C-C	S-S	C-S	Terminal-inner	Inner-inner
	C3-C16' 3.451 C6-C14' 3.405 C7-C13' 3.495 C8-C11' 3.486 C11-C8' 3.486 C13-C7' 3.495 C14-C6' 3.405 C16-C3' 3.451	S2-S6' 3.706 S3-S5' 3.721 S5-S3' 3.721 S6-S2' 3.706	C4-S6' 3.598 S6-C4' 3.598	C8-C7-C9-C10 –77.6(3) C5-C7-C9-C11 –88.7(4)	C16-C15-C15'-C16' –77.12 C13-C15-C15'-C13' –88.44
Compound	Distances between [7]helicene moieties[b]			Torsion angles for β,β-linkages	
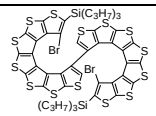 *MRM*	C-C	S-S	C-S	Within [7]helicene moieties	Between [7]helicene moieties
	C2-C16' 3.226 C16-C2' 3.226 C5-C13' 3.296 C7-C11' 3.250 C9-C9' 3.297 C11-C7' 3.250 C13-C5' 3.296	S1-S7' 3.879 S2-S6' 3.856 S3-S5' 3.743 S4-S4' 3.742 S5-S3' 3.743 S6-S2' 3.856 S7-S1' 3.879	C3-S7' 3.459 S7-C3' 3.459	C8-C7-C9-C10 –11.68 C5-C7-C9-C11 –25.93	C16-C15-C15'-C16' –50.14 C13-C15-C15'-C13' –51.16

[a] For tetrakis(β-trithiophene) **1**, all C-C and C-S distances listed in the Table are below the sum of the van der Waals radii plus 0.1 Å. [b] For bis[7]helicene **2**, all C-C and C-S distances listed in the Table are below the sum of the van der Waals radii.

Table S2. Summary of chiral HPLC results for tetrakis(β-trithiophene) **1** and bis[7]helicene **2**.

Compound	HPLC label	No.	Compound label	Solvent system		Left peak	Right peak	HPLC plot
				Hexane	*i*-PrOH	(%)	(%)	
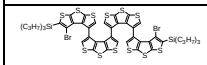	MM-19-71-solid	1 2	MM-19-71-solid	99.5 99.5	0.5 0.5	55.22 56.18	44.78 43.82	***Figure S8***
	MM-20-92-1	1	Reference ([11]helicene)	99.5	0.5	46.56	53.44	
	MM-19-39-1	1 2	MM-18-26+29-f2 +f1-B	100 100	- -	57.91 58.49	42.09 41.51	
	MM-19-39-2	1 2	MM-19-25+28-col -2-solid	100 100	- -	57.64 58.04	42.36 41.96	***Figure S7***
	MM-18-59-TP2	1 2 3 4	MM-18-59-TP2	99 99 100 100	1 1 - -	single single 26.91 25.67	peak peak 73.09 74.33	***Figure S9*** ***Figure S10***
	MM-19-60-1	1	Reference ([7]helicene)	100	-	51.89	48.11	
	MM-19-60-2	2 3	MM-19-48+53-TP 1	100 100	- -	37.01 37.17	62.99 62.83	***Figure S11***
	MM-19-57-TP2	1 2	MM-19-57-TP2	99.5	0.5	34.33 34.01	65.67 65.99	(some impurities)
	MM-20-92-1	1	Reference ([11]helicene)	99.5	0.5	46.56	53.44	
	MM-20-96-solid	1	MM-20-96-solid	100	-	44.23	55.77	
	MM-20-98-1	1	Reference ([7]helicene)	100	-	51.03	48.97	
	MM-21-40-1	3	Reference ([7]helicene)	100	-	51.11	48.89	***Figure S12***
	MM-21-15-solid	1 2	MM-21-15-TP3-A +B-1+2-TP1-solid	100	-	19.05 15.74	80.95 84.26	***Figure S13***
	MM-21-26-A-2	1 2	MM-21-26-TP2+T P3-A-2	100	-	16.02 15.87	83.98 84.13	***Figure S14*** (PTLC- purified)
	MM-21-26-solid	1 2	MM-21-26-TP2+T P3-A-4+5-solid	100	-	52.29 52.83	47.71 47.17	***Figure S15*** (remaining on plate)

Table S3. Summary of ^{1}H NMR experiments with chiral shift reagents for tetrakis(β-trithiophene) **1** and bis[7]helicene **2**.

Compound structure Sample label	Mass (mg)	NMR label	Yb(hfpc) (mg)	Ag(fod) (mg)	LB/GB (Hz)	Chemical shift of ^{1}H NMR in aromatic region (integration)	Comment
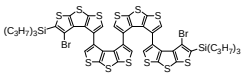 MM-19-25+28-col-2-solid (***Figure S16***)	0.8	MM-19-25+28-col-2-solid	—	—	0.3/0	7.045, 6.706, 6.237	
		MM-19-25+28-col-2-solid	0.8	1.2		7.056, 7.051, 6.715 (not split), 6.240 (not split)	
		MM-19-25+28-col-2-solid	0.8	1.2		7.055, 7.050, 6.714 (not split), 6.239 (not split)	(re-shimmed)
		MM-19-25+28-col-2-solid	0.8+1.4	1.2+1.5	–0.8/0.4	7.074 (1.0 H), 7.054 (0.96 H), 6.726 (1.03 H), 6.721 (1.03 H), 6.242 (0.99 H), 6.233 (0.99 H)	
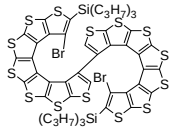 MM-19-57-TP2 (***Figure S17***)	~0.3	MM-19-57-TP2-$CDCl_3$	—	—	0.3/0	7.025	
		MM-19-57-TP2-1	1.1	1.3	–0.5/0.3	7.042 (1.0 H), 7.036 (1.37 H)	
		MM-19-57-TP2-2	1.1+2.6	1.3+2.8	–0.6/0.3	7.088 (1.0 H), 7.070 (1.21 H)	(shimming?)
		MM-19-57-TP2-3	1.1+2.6	1.3+2.8	–0.6/0.3	7.086 (1.0 H), 7.069 (1.17 H)	(7.8% ee)
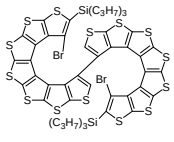 MM-19-48+53-TP1 (***Figure S18***)	0.4	MM-19-59-1	—	—	0.3/0	7.025	
		MM-19-59-2	0.7	1.2	–0.8/0.4	7.043 (1.0 H), 7.038 (1.27 H)	(12% ee)
		MM-19-59-3	0.7+1.2	1.2+0.8	–0.8/0.4	7.058 (1.0 H), 7.049 (1.84 H, overlapped with ^{13}C satellite)	
		MM-19-59-4	0.7+1.2+0.9	1.2+0.8+1.0	–0.8/0.4	7.070 (1.00 H), 7.060 (1.17H)	(7.8% ee)

Table S4. B3LYP/6-31G(d) geometry optimizations and vibrational frequency calculations for Br- and TMS-terminated carbon-sulfur [*n*]helicenes and bis[7]helicenes.

	Bis[7]helicene **2a**-*MM*	Bis[7]helicene **2a**-*PM*		[15]Helicene **3a**	[7]Helicene **5**
Point group	C_2	C_1	C_i	C_2	C_2
Torsion angle (outer/inner)[a]	-52.2/-49.8[h]	175.0/175.7	180.0/180.0	-11.9/-15.2	-
Total energy[b]	-12757.0879517	-12757.0753497	-12757.0753501	-13154.0582402	-9358.9360643
RMS gradient norm[c]	1.70e-06	1.97e-06	8.20e-07	7.00e-07	1.03e-06
Maximum force[c]	0.000005921	0.000008132	0.000001906	0.000001975	0.000003668
Zero-point-energy[d]	290.14984	290.37343	290.24331	277.55846	209.42599
Relative energy[d,e]	0	8.13	8.00	-	-
Vibrational frequencies[f]	10.5, 19.1, 21.9	5.5, 14.3, 20.3	*i*2.2, 12.5, 19.0	15.9, 17.0, 25.7	26.0, 33.5, 36.1
Dipole moment[g]	2.44	0.26	0.00	1.49	1.67
Br-Br (Å)	7.25[h]	7.40	7.40	7.22	-
terminal S-S (Å)	11.05[h]	10.98	11.02	10.86	-
Total energy (in uahf cyclohexane)[b]	-12757.0889289	-	-12757.0762607	-13154.0591076	-9358.93673347
Relative energy (in uahf cyclohexane)[d,e]	0	-	7.949	-	-
Dipole moment (in uahf cyclohexane)[g]	2.68	-	0.00	1.65	1.83

[a] CCCC torsion angle (°) between the [7]helicene units; the inner angle is defined by the four center carbons on the inner helix and the outer angle is defined by the four carbons for the center thiophene ring in [15]helicene or the corresponding four carbons in bis[7]helicene. [b] In Hartree/molecule. [c] In a.u., Cartesian coordinates. [d] In kcal mol^{-1}, unscaled. [e] Relative energy with respect to **2a**-*MM*. [f] Three lowest frequencies in cm^{-1}. [g] Dipole moment in Debeye. [h] The corresponding values determined from the X-ray structure of **2**: -50.1° (outer), -51.2° (inner), 6.90 Å (Br-Br), and 11.24 Å (terminal S-S).

Table S5. B3LYP/6-31G(d,p) geometry optimizations and vibrational frequency calculations for hydrogen-terminated carbon-sulfur bis[7]helicenes, tris[7]helicenes, and tetrakis[7]helicenes.

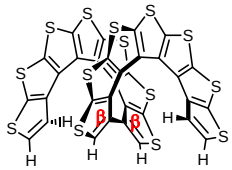
bis[7]helicene **6**-*MM*

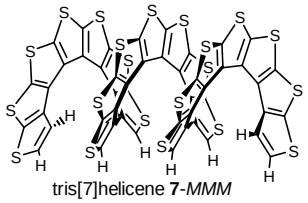
tris[7]helicene **7**-*MMM*

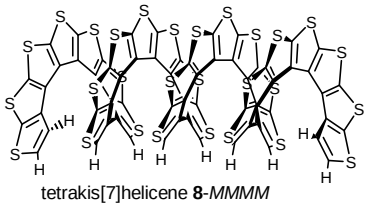
tetrakis[7]helicene **8**-*MMMM*

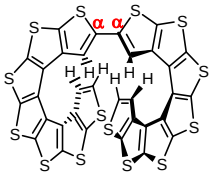
bis[7]helicene **9**-*MM*

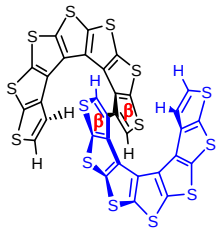
bis[7]helicene **6**-*PM*

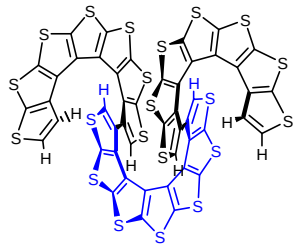
tris[7]helicene **7**-*MPM*

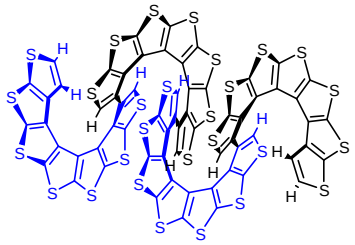
tetrakis[7]helicene **8**-*MPMP*

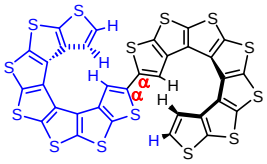
bis[7]helicene **9**-*PM*

Linkage	Oligomer	Point group	Torsion angles[a]	Total energy[b]	RMS gradient norm[c]	Zero point energy[d]	Relative energy[d,e]	Vibrational frequency[f]	Dipole moment[g]
β,β	**6**-*MM*	C_2	-51.8	-6797.53316673	1.20e-06	174.99	0	11.2, 24.8, 35.4	1.81
β,β	**6**-*PM*	C_i	180.0	-6797.52426336	1.90e-06	174.94	5.54	2.3, 18.9, 32.4	0.0
β,β	**7**-*MMM*	C_2	-53.8, -53.8	-10195.6858842	7.84e-07	255.94	0	9.9, 16.7, 21.1	2.26
β,β	**7**-*MPM*	C_2	172.3, 172.3	-10195.6656715	7.36e-07	255.92	12.70	5.1, 8.2, 14.5	1.20
β,β	**8**-*MMMM*	C_2	-54.1, -55.9, -54.1	-13593.8382720	7.83e-07	336.75	0	7.3, 12.6, 15.8	2.69
β,β	**8**-*MPMP*	C_i	171.9, 180.0, -171.9	-13593.8060036	1.38e-06	336.86	20.36	3.2, 5.9, 7.1	0.0
α,α	**9**-*MM*	C_2	-32.4	-6797.56029703	2.12e-07	175.27	0	5.9, 13.1, 13.3	0.59
α,α	**9**-*PM*	C_i	180.0	-6797.56184080	1.61e-06	175.18	–1.05	*i*5.2, 13.8, 19.3	0.0

[a] (H)CCCC(H) torsion angles (°) between the [7]helicene units. [b] In Hartree/molecule. [c] In a.u., Cartesian coordinates. [d] In kcal mol^{-1}, unscaled. [e] Energy difference between diastereomers relative to the energy of the "homochiral" diastereomer. [f] Three lowest frequencies in cm^{-1}. [g] Dipole moment in Debeye.

5. Supporting References.

S1. J. Suffert, *J. Org. Chem.* **1989**, *54*, 509–510.

S2. SADABS: R. Blessing, *Acta Cryst. A* **1995**, *51*, 33–38.

S3. SAINT 6.1, Bruker Analytical X-Ray Systems, Madison, WI, 1999.

S4. Sir2004, A Program for Automatic Solution and Refinement of Crystal Structure, M. C. Burla, R. Caliandro, M. Carnalli, B. Carrozzini, G. L. Cascarano, L. De Caro, C. Giacovazzo, G. Polidori, R. Sagna, Version 1.0, 2004.

S5. SHELXL-97: SHELXTL-Plus V5.10, Bruker Analytical X-Ray Systems, Madison, WI.

S6. A. Rajca, M. Miyasaka, M. Pink, H. Wang, S. Rajca, *J. Am. Chem. Soc.* **2004**, *126*, 15211−15222.

S7. M. Miyasaka, A. Rajca, M. Pink, S. Rajca, *J. Am. Chem. Soc.* **2005**, *127*, 13806−13807.

S8. M. J. Frisch, G. W. Trucks, H. B. Schlegel, G. E. Scuseria, M. A. Robb, J. R. Cheeseman, J. A. Montgomery Jr., T. Vreven, K. N. Kudin, J. C. Burant, J. M. Millam, S. S. Iyengar, J. Tomasi, V. Barone, B. Mennucci, M. Cossi, G. Scalmani, N. Rega, G. A. Petersson, H. Nakatsuji, M. Hada, M. Ehara, K. Toyota, R. Fukuda, J. Hasegawa, M. Ishida, T. Nakajima, Y. Honda, O. Kitao, H. Nakai, M. Klene, X. Li, J. E. Knox, H. P. Hratchian, J. B. Cross, C. Adamo, J. Jaramillo, R. Gomperts, R. E. Stratmann, O. Yazyev, A. J. Austin, R. Cammi, C. Pomelli, J. W. Ochterski, P. Y. Ayala, K. Morokuma, G. A. Voth, P. Salvador, J. J. Dannenberg, V. G. Zakrzewski, S. Dapprich, A. D. Daniels, M. C. Strain, O. Farkas, D. K. Malick, A. D. Rabuck, K. Raghavachari, J. B. Foresman, J. V. Ortiz, Q. Cui, A. G. Baboul, S. Clifford, J. Cioslowski, B. B. Stefanov, G. Liu, A. Liashenko, P. Piskorz, I. Komaromi, R. L. Martin, D. J. Fox, T. Keith, M. A. Al-Laham, C. Y. Peng, A. Nanayakkara, M. Challacombe, P. M. W. Gill, B. Johnson, W. Chen, M. W. Wong, C. Gonzalez, J. A. Pople, *Gaussian 03*, Revision E.01 (Gaussian, Wallingford, CT, 2004).

S9. J. Zheng, B. J. Lynch, Y. Zhao, D. G. Truhlar, Database of Frequency Scaling Factors for Electronic Structure Methods, http://comp.chem.umn.edu/database/freq_scale.htm.

S10. A. P. Scott, L. Radom, *J. Phys. Chem.* **1996**, *100*, 16502–16513.

S11. J. Tomasi, B. Mennucci, R. Cammi, *Chem. Rev.* **2005**, *105*, 2999–3094.

S12. A. V. Marenich, R. M. Olson, C. P. Kelly, C. J. Cramer, D. G. Truhlar, *J. Chem. Theory Comput.* **2007**, *3,* 2011–2033.